Electro-Optical Characterization of Passivated InAsP/InP Quantum Discs-in-Nanowire Heterostructures

Student:
Samareh Kordi Jazi

Supervisor:
Håkan Pettersson

LUND
UNIVERSITY

Lund
December 2018

Table of contents

Acknowledgement

First of all, I would like to express my sincere gratitude to my main supervisor, Prof. Håkan Pettersson. I must thank you for giving me the chance to work in this attractive and challenging project which provided me the opportunity to learn about semiconductor devices and their applications, how to do research and how to collaborate in scientific work. Also, I thank you for being available for guidance and help.

Second, I would especially like to thank Prof. Mats-Erik Pistol for his inspiring and insightful advices during the whole project and also for guiding me through this interesting project. Mats-Erik, thank you for giving me the opportunity to work with the PL set-up which helped me not only to learn optics but also to understand how a research project can be completed in reality.

I would also like to thank my co-supervisor, Mohammad Karimi. You have always been helpful from the beginning of the project until the very end. Without your responsible assistance, I could not have finished my thesis work. The discussions with you were always great and I learnt a lot.

Irene Geijselaers, I am deeply grateful for your patience and for the amount of time you spent in the lab teaching me PL spectroscopy, alignment skills and being my experimental mentor. It was a lot of work for you and I appreciate your friendliness.

A big thanks also to our sample grower Xulu Zeng for his collaboration despite his limited time due to his PhD defense. Also, big thanks to Lukas Hrachowina for doing electrical measurements. I would also like to thank Neimantas Vainorius for sharing his expertise about the PL setup.

Great thanks to NanoLund in general for providing us with such a great facility for doing research, and to all my colleagues and friends who supported me during my studies.

Abbreviations

NW	Nanowire
IR	Infrared
LED	Light emitting diode
PL	Photoluminescence spectroscopy
QDisc(s)	Quantum disc(s)
QW	Quantum well
MOVPE	Metal organic vapor phase epitaxy
NP	Nano particle
TMIn	Trimethylindium
EBL	Electron Beam Lithography
NIL	Nanoimprint lithography
SEM	Scanning electron microscopy
CB	Conduction band
VB	Valence band
ZB	Zincblende
WZ	Wurtzite

Abstract

Semiconductor nanowires, with their quasi one-dimension geometry, inherently provide strain relaxation for heterogeneous integration and also strong light mode confinement. Nanowire-based photonic devices have also been demonstrated to offer significantly enhanced quantum efficiency, gain and reduced noise. This project deals with electro-optical investigations of InP nanowires with axially embedded InAsP quantum discs. The advantages of InP/InAsP nanowire-based photodetectors include direct growth on lattice-mismatched silicon platforms due to the small nanowire footprint, significant bandgap tuning, strong confinement in quantum discs and optical resonances providing a large optical absorption despite the small material volume compared to a thin film. However, due to the large surface-to-volume ratio of nanowires, surface states can strongly affect the electro-optical performance of nanowire-based heterostructure devices. Surface states can induce e.g. Fermi-level-pinning, non-radiative recombination and significant surface leakage currents which can deteriorate the performance of nanowire-based devices. Despite of all passivation attempts, surface states are still a challenge for InP/InAsP nanowire heterostructures. In this thesis work, the surfaces of InP nanowires, with embedded single- or 20 InAsP quantum discs, were passivated using atomic layer deposition of SiO_2 or PO_x/Al_2O_3. Single passivated nanowires were optically characterized by photoluminescence and the results were compared with as-grown nanowires. To evaluate the effect of passivation on the corresponding electrical properties of the nanowires, nano-probe current-voltage measurements were carried out on single nanowires still standing on the growth substrate. Our results show that passivation with PO_x/Al_2O_3 improves the optical properties of the nanowires. PO_x/Al_2O_3 passivation leads to improved electrical characteristics in the nanowires with 20 quantum discs, while SiO_2 enhances the electrical properties of nanowires with a single embedded quantum disc. The results will be used for future optimization of photodetectors.

1 Introduction

Human interest to explore new phenomena has motivated researchers to probe systems with extremely small sizes. This trend has led to the birth of nanoscience and to the development of fascinating nanoscale devices. One type of nanomaterials is semiconductor nanowires (NWs). NWs are quasi-one-dimensional structures with a length in the range of microns and a diameter of the order of ten to one hundred nanometers. These nanostructures have demonstrated great potential in nanophotonic and optoelectronics devices such as solar cells [1], photodetectors [2] and light-emitting diodes (LED) [3]. Due to the small footprint of III-V NWs, they can be grown directly on commercial Si substrates [4], which is otherwise impossible due to significant lattice mismatch [5]. Moreover, photonic resonances in periodic arrays of NWs can be tailored by altering the geometrical properties such as length, diameter and pitch [6]. Also, due to the low thermal budget in NW growth, they can potentially be monolithically integrated with mature Si CMOS technology [7] which is very important for future integration of highly efficient [8] optoelectronic devices with read-out and processing integrated electronics [1] [2] [9]. Nanowire-based photodetectors have been shown to be a good alternative to commercially available conventional photodetectors [5] [10] [11], due to the possibility to grow defect-free lattice-mismatched heterostructures which offer a broader spectral detection range [12] [13]. Moreover, GaAs NW-based solar cells with an efficiency of 15.3 % [14] have shown to be a strong competitor to bulk solar cells. Nanowire-based transistors without junction [15], Schottky diodes based on single GaN NWs [16] and radial AlGaInP NW-based light emitting diodes [17] are merely some examples of NW-based devices which are based on NWs.

By embedding quantum heterostructures inside the NWs, one could benefit from both properties of the NWs themselves, and from additional tunable properties related to the discrete energy structure and confinement of carriers in the quantum structures. Highly efficient InGaN/GaN quantum dots in NW LEDs [18], room-temperature NW lasers with multiple radial GaAs/AlGaAs quantum wells (QWs) [19] and long-wavelength infrared (IR) photodetectors based on InAsP quantum discs (QDiscs) embedded in InP NWs are just some examples of optoelectronic devices made with NW heterostructures [20].

Heterostructure NWs can also be grown directly on Si substrates for the same reason stated above. NW heterostructure-based devices have shown a significant enhancement in quantum efficiency [8] and decrease in noise [21]. Due to all benefits, NW-based devices are serious competitors to silicon-based devices.

Besides all the advantages that NWs can introduce in electronics and photonics they suffer from issues which seriously decrease their efficiency. One significant detrimental effect has to do with NW surface states. Due to the large aspect ratio of NWs, and thus large surface-to-volume-ratio, the amount of leakage current and non-radiative surface recombination can be substantial [22]. Moreover, the surface states scatter the charge carriers causing a reduction in conductivity [23]. The depletion layer caused by surface states can extend through the whole interior of thin NWs [24] [25] which affects their photo-electrical properties [26]. Hence, the passivation of

the NW surface is a critical step for high-performance optoelectronic device applications. There have been some reports on passivation of the surfaces of NWs using different techniques. For instance, Münch et al. reported that atomic layer deposition (ALD) of HfO_2 can enhance the surface properties of InP NWs, regardless of any pretreatment or deposition condition [27]. Dhaka et al. evaluated the effect of ALD deposition of Al_2O_3, AlN, TiN, GaN and TiO_2 layers on InP NWs and observed enhanced surface properties [28]. Zhong et al. also reported on an increase in PL intensity and lifetime by deposition of a layer of SiN_x using plasma-enhanced chemical vapor deposition (PECVD) on InP NWs [29]. Recently, Black et al. reported on surface passivation of InP NWs using ALD deposition of PO_x, followed by a layer of Al_2O_3 [30]. They observed an enhancement of PL by a factor of 20 at low excitation power with long-term stability of around 7 months and thermal stability at elevated temperatures (>300 °C). Although these results are promising for passivating the surface of InP NWs, to the best of our knowledge there are no reports on surface passivation of InP NWs with embedded quantum heterostructures.

In this work, we focus on the passivation of InP NWs with embedded InAsP quantum heterostructures. InP NWs are regarded as a promising candidate for optoelectronic devices due to their high electron mobility and direct band gap of around 1.4 eV, which is suitable for photovoltaic applications and also for integration with other III-V semiconductor compounds. Although it is reported that InP NWs offer low surface recombination velocity of 10^2 to 10^4 cm/s depending on the doping concentrations [31] [32] [33] [34], this velocity is still a limiting factor for many InP NW-based devices. InP/InAsP heterostructures have attracted great interest due to their high electron mobility [30] which can be employed for making high-speed electronic devices [35] [36]. Also, due to the large band edge offsets between InP and InAsP, carrier confinement is strong enough to increase the operating temperature in lasers and to reduce the leakage current in detectors [7]. Three sets of InP NW samples with single- or multiple InAsP QDiscs were prepared for passivation. In each set, one sample was passivated by ALD of SiO_2using the Savanah setup in Lund NanoLab, one sample was passivated by ALD of PO_x/Al_2O_3using the Fiji setup and one sample was kept as-grown. Current-voltage (I-V) characterization of each sample, with and without electron beam illumination, was carried out by using an in-situ nanoprobe tool in a SEM, while spectrally resolved optical characterization was performed using PL spectroscopy (this part was done by myself). Chapter 2 provides a brief theoretical background to the studied samples. Chapter 3 describes the techniques for growing InP/InAsP heterostructure NWs and the ALD passivation method invoked to improve the NW properties.
Chapter 4 explains the characterization methods which were used in this project i.e., in-situ nano-probe IV characterization and PL. The results of the IV and PL measurements are discussed in Chapter 5, followed by a summary of this work together with some future plans in Chapter 6.

2 Basic theory

2.1 The p-n junction

The p-n junction is formed when a p-doped semiconductor is merged with an n-doped semiconductor. The key feature of p-n junctions is that they can rectify; i.e., they allow the current to flow in one direction (forward bias) and block the current in opposite direction (reverse bias). Figure 1 shows the current-voltage characteristics of a typical p-n junction.

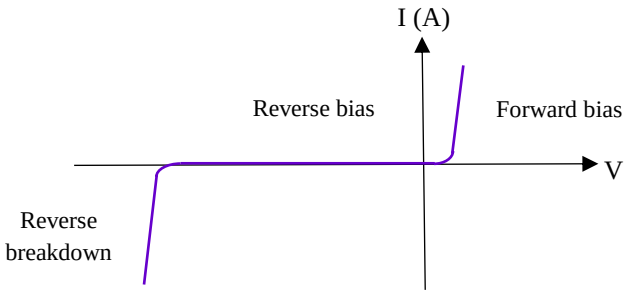

Figure 1: The I-V characteristic of a typical p-n junction

When a forward bias is applied to the junction, i.e., a positive bias is applied to the p-side, the current flows and increases exponentially with bias. If a reverse bias is applied, i.e., a negative bias is applied to the p-side, only a small saturation current flows below a critical voltage, called the breakdown voltage, beyond which the current increases abruptly.

Figure 2 shows a schematics of the band diagram of a p-n junction. Without applied bias and illumination (thermal equilibrium), the Fermi level is close to the valence band of the p-type semiconductor and to the conduction band of the n-type semiconductor.

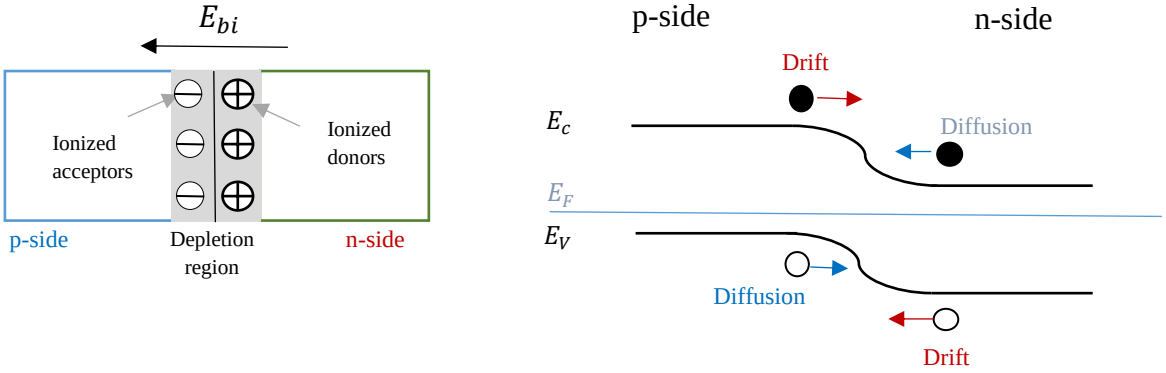

Figure 2: Left figure shows the schematic layout of a p-n junction with indicated space charge and built-in electric field. Right figure shows the band diagram of a p-n junction where the flow of electrons (dark circles) and holes (white circles), due to drift and diffusion, are shown.

When two p- and n-type semiconductors are joined together, a carrier concentration gradient forms at the interface. This gradient causes charge carriers to diffuse; i.e., the holes tend to diffuse from the p-side to the n-side and the electrons diffuse from the n-side to the p-side, creating a diffusion current. When a hole diffuses into the n-side, it leaves behind a negative acceptor ion. Similarly, when an electron diffuses into the p-side, it leaves behind a positive donor ion. These positive and negative ions are left uncompensated, which leads to the formation of a negative space charge on the p-side and a positive space charge on the n-side, as shown in Fig. 2. This space charge results in an electric field and thus a drift mechanism that counteracts the diffusion mechanism. In thermal equilibrium, a depleted space charge region is formed hosting a built-in electric field, E_{bi}, pointing from the n- region to the p-region. With applied bias, the current through a p-n junction is given by:

$$I = I_0(e^{\frac{qV}{\eta kT}} - 1)$$

Here, I and V is the diode current and applied bias, respectively. I_0 is the saturation current, T is the operating temperature, k is the Boltzmann constant and q is the electron charge. The so called ideality factor η depends on the detailed current generation mechanisms. If η=1 the diode is said to be ideal and diffusion-driven. If the current generation is instead governed by recombination processes the value of η is 2. At room temperature, T=300°K, $\frac{kT}{q} = 25.85\ \text{mV}$ which is called thermal voltage. Typically, the ideality factor for a diode has a value between 1 and 2.

We can consider two important cases:

- For a reverse (negative) bias $|V| >> \left|\frac{kT}{q}\right| = 26\text{mV}$ at 300K: $I = -I_0$
- For a forward (positive) bias $V >> \frac{kT}{q} = 26\text{mV}$: $I = I_0 e^{\frac{qV}{\eta kT}}$

For finding I_0 and η, the current can be measured as a function of applied forward bias and then plotted in a semi-log format according to:

$$\ln I = \ln I_0 + \frac{q}{\eta kT} V$$

From a linear fit of this expression, it is possible to extract I_0 from the intercept of the extrapolated line with the y-axis, whereas the slope of the line yields η.

2.2 Photocurrent generation in p-n junctions

If a semiconductor is illuminated by a photon with an energy larger than the bandgap energy (the energy difference between the conduction band (CB) and the valence band (VB)), an electron-hole pair is generated. If the electron-hole pairs are generated inside the depletion region, or within a diffusion length away from it, they are separated by the built-in electric field which generates a photocurrent in an external circuit as shown in Fig.3 below. In order to collect more electrons and holes, it is useful to make the depletion region wider. There are some

approaches to increase the depletion region. By applying a reverse bias, the width of the depletion region and electric field also increases. Another possibility to realize an extended depletion region is to incorporate an intrinsic (undoped) region between the p- and the n-regions.

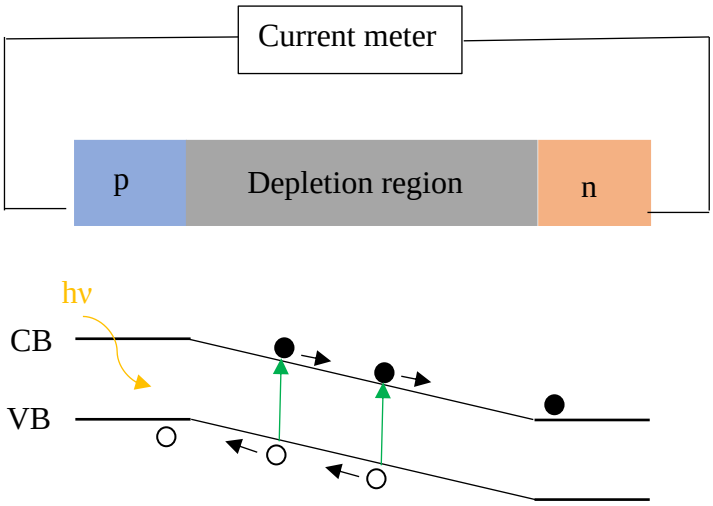

Figure 3: The band diagram of a p-n junction in a NW under illumination

2.3 Heterostructures

When two semiconductors with different bandgaps are merged, three types of the band alignment can take place as schematically shown in Fig. 4. The type-I band alignment forms when the narrow bandgap of one constituent semiconductor is energetically enclosed within the wider bandgap of the other semiconductor. The two other band alignments, type II, or staggered alignment, and type III or broken alignment, are also depicted in Fig. 4.

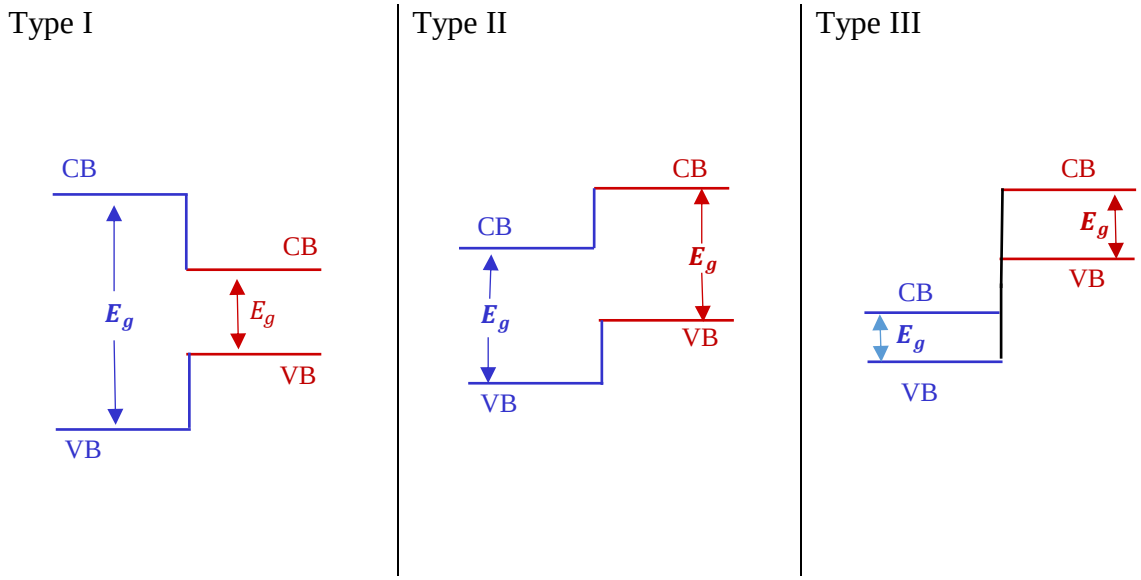

Figure 4: Three types of band alignment

It should be noted that a type-II interface is formed between ZB InP and WZ InP. It is reported [37] that the valence band and the conduction band edges of WZ InP are 45 meV and 120 meV higher, respectively, than those of the ZB InP.

2.4 The quantum well

A quantum well (QW) is formed by sandwiching a thin semiconductor layer, with thickness of the order of the de Broglie wavelength, in between two semiconductors with a different bandgap such that the charge carriers (electron or holes) are confined to the thin layer. This confinement results in a discretization of the energy structure and to the formation of subbands. The emission of light from QWs typically results from interband transitions between subbands in the CB and VB, but can also take place in intersubband transitions between different subbands in the CB (or VB). If QWs are excited with a high interband intensity, lower energy states are filled which results in a blueshift of the PL signal [38].

In QW photodetectors, a photocurrent is generated when incoming radiation excites interband or intersubband transitions. The excited charge carriers are subsequently escaping from the QW to the barrier material under the influence of thermal excitation and applied electric field. Since intersubband transitions typically involve low energy photons, QW photodetectors are sensitive to long wavelength infrared radiation.

2.5 Band structure of NW samples

All samples (InP NWs) studied in this project have three different segments as shown in Fig. 5. The bottom segment is n^+, the middle segment is intrinsic (i), and the top segment is again n^+ The QDs were grown inside the intrinsic segment. The substrate is always p+.

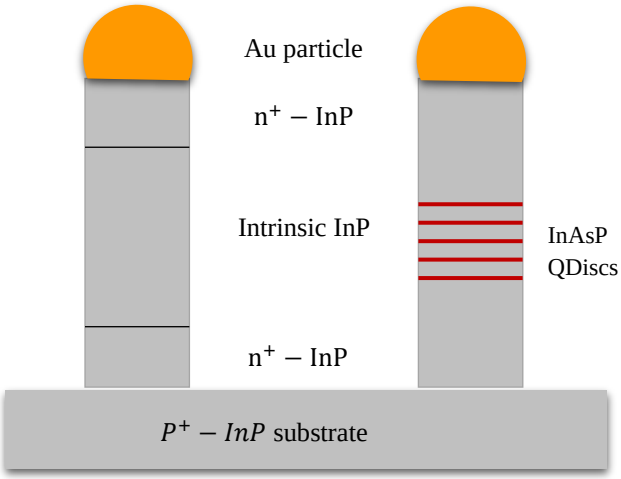

Figure 5: Schematic of the doping profile of the investigated InP NWs with axial embedded InAsP QDiscs.

During the growth process, the intrinsic part becomes unintentionally weakly n-doped due to the "reactor memory effect" or "particle reservoir effect". Residual n-precursors remain inside the reactor after switching off the precursor supply, which causes undesired doping in the subsequent growth. For instance, TESn was applied for the growth of the n-segment in the InP NWs. Due to the memory effect, this precursor causes unintentional n-doping of the nominally intrinsic part. The reservoir effect is another factor caused by high element solubility in the seed particle. In our case, Sn has high solubility in the Au seed particle [39], so there is some amount of Sn left in the metal seed particle even after the Sn precursor is turned off.

The unintentional n-doping in the intrinsic segment affects the NW properties. In order to improve the investigated NW–based detector performance, Zn is introduced intentionally in a molar fraction of 0.5×10^{-7} (it is the optimum amount of Zn based on the Ref. [7]) to compensate the n-doping in the intrinsic part. Results that are shown in Ref. [7] proves that in-

situ-Zn doping reduces the dark current and leads to excellent performance of NW-based photodetectors.

The NWs have zincblende (ZB) and wurtzite (WZ) crystal structures inside the intrinsic segment, as shown in the following TEM image, Fig. 6:

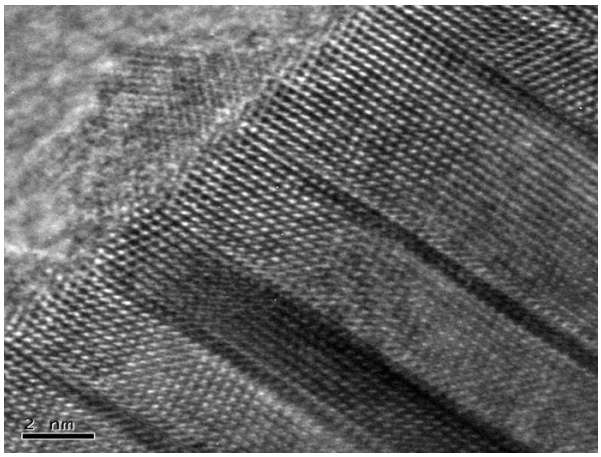

Figure 6: TEM image shows ZB and WZ regions in the intrinsic part of the NW. The dark area shows the ZB segments while the light area shows the WZ segments.

The schematic energy band structure of the samples is shown in Fig. 7. In the highly p-doped substrate the Fermi level $E_F$is inside the VB, whereas E_F is located in the CB for the highly n-doped InP segments. A highly doped p-n junction is formed in the bottom part of the NW. The bandgap energy, E_g, of InP varies between 1.493-1.5 eV at 4 K for the WZ crystal structure and between 1.413-1.416 eV for the ZB crystal structure [40] [37]. The bandgap energy for $InAs_{0.45}P_{0.55}$ is expected to be between 0.86-0.96 eV [41] [20].

As seen in Fig. 4, InP / InAsP heterostructures form a type-I alignment. The CB offset is about 0.35 eV [42] and the VB offset is in the range of 0.20 eV. The discontinuities between the CB and the VB form a potential well which can trap both electrons and holes. Electrons and holes are free to move in two directions, but they are confined along the growth direction of the QW. The corresponding electronic structure comprises subbands inside the QW as shown by green lines in Fig. 7.

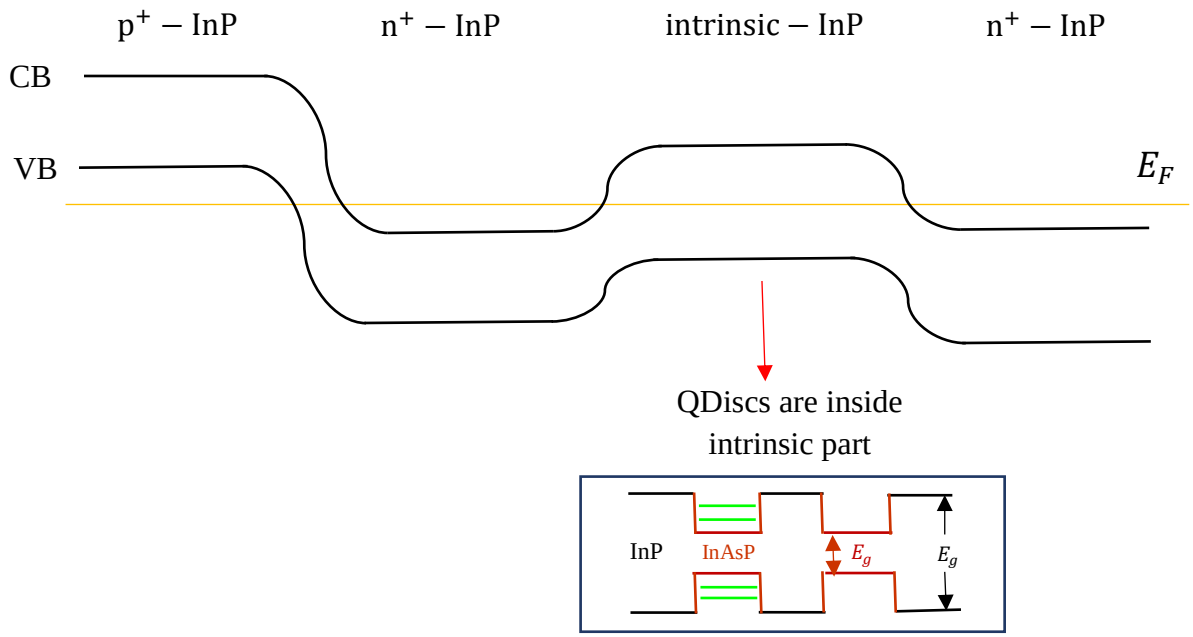

Figure 7: The schematic energy band diagram of an n+-i-n+ InP NW grown on a p+ InP substrate. The inset shows the band diagram in the intrinsic region which includes QDiscs. The confined subbands are shown by green solid lines in the QW (Appendix A).

3 Growth and passivation of axial InAsP/InP NW heterostructures

3.1 Sample preparation

3.1.1 Nanowire growth

Semiconductor NWs can be fabricated by different methods which can be categorized into two approaches: top-down and bottom-up approaches. The top-down technique is a subtractive method like carving a statue from large bulk materials. It employs a large number of techniques like lithography and chemical etching to make NWs from a bulk material. The size of the smallest object that can be produced by this method is limited by the lithography resolution and etching parameters. This method has obvious disadvantages such as complicated fabrication techniques with expensive equipment and time-consuming processing. One important drawback is that it cannot be used to fabricate semiconductor heterostructures with significant lattice-mismatched materials (like InP/InAs) which makes it unfavorable for synthesis of NW heterostructures.

In contrast to the top-down approach, the bottom-up method is an additive technique where atoms add together to form much larger complex structures. The bottom-up approach is usually carried out by epitaxial growth which is a highly controllable method for fabrication of heterostructures with atomic-scale precision. There are several methods for layer-by-layer epitaxial growth such as molecular beam epitaxy (MBE), liquid-phase epitaxy (LPE) and metal-organic vapor phase epitaxy (MOVPE). Among them, MOVPE and MBE are prevalent techniques for epitaxial growth of heterostructure NWs. In MOVPE, some precursors containing the desired elements are injected into the growth chamber. At a proper temperature and pressure, the structure can be grown.

The samples used in this work are InP NWs with single or 20 axially embedded $InAs_{0.45}P_{0.55}$ QDiscs, grown by MOVPE in vertical arrays on InP substrates. Trimethylindium (TMIn) and phosphine (PH_3) are used as precursors injected into the growth reactor. For growing the NWs by MOVPE, the substrate should be patterned by metal seed nanoparticles (NP) like Gold (Au) which act as catalysts to start the growth process.

The substrates in this work are p^+-InP(111)B patterned by nanoimprint lithography (NIL). In NIL, the surface of the substrate is coated with resist layers and an intermediate polymer stamp (IPS) is used to pattern these resist layers under special conditions with thermal/pressure cycles, followed by the UV illumination. After cleaning, the substrates undergo a metal evaporation step followed by a lift-off process to remove the residual resist layers. The lift-off process leads to a final design including Au NPs with 180 nm diameter and 20 nm thickness, periodically arranged with 400 nm center-to-center distance (pitch). Figure 8 shows a SEM image of a substrate which is patterned by Au NPs.

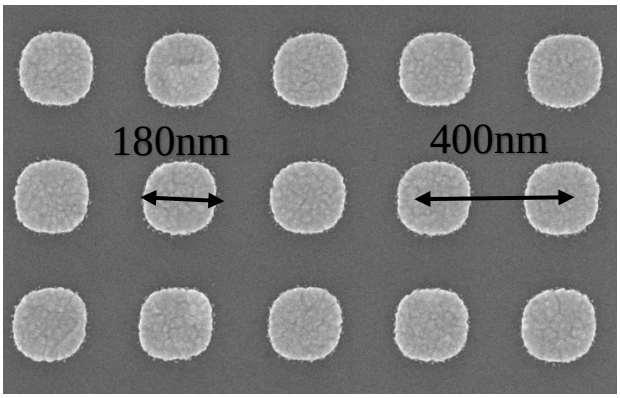

Figure 8: Top view of patterned InP substrate with ordered Au seed NPs.

For growing the NWs, the MOVPE system is operated at low pressure of 100 mbar and a temperature of 440℃. The grown NWs have a diameter of 130 nm and a length of 2 μm. If during the growth process, the precursor TMIn is turned off and PH_3 is replaced by AsH_3 for 2 seconds [43] [44], the heterostructure InAsP QDiscs can be grown. During the growth of the QDiscs, In is supplied from the NPs due to the reservoir effect. Since some elements, in particular group III elements like Al, Ga, and In [45], are more soluble in the metal seed particles (Au NPs in this work), they can act as the reservoir of those elements. To continue the growth of the InP NWs, AsH_3 is turned off and the TMIn precursor is again injected into the growth chamber. For growth of multiple QDiscs, this process described above is repeated until the desired number of InAsP/InP QDiscs is grown. Figure 9 shows the schematic of the growth process.

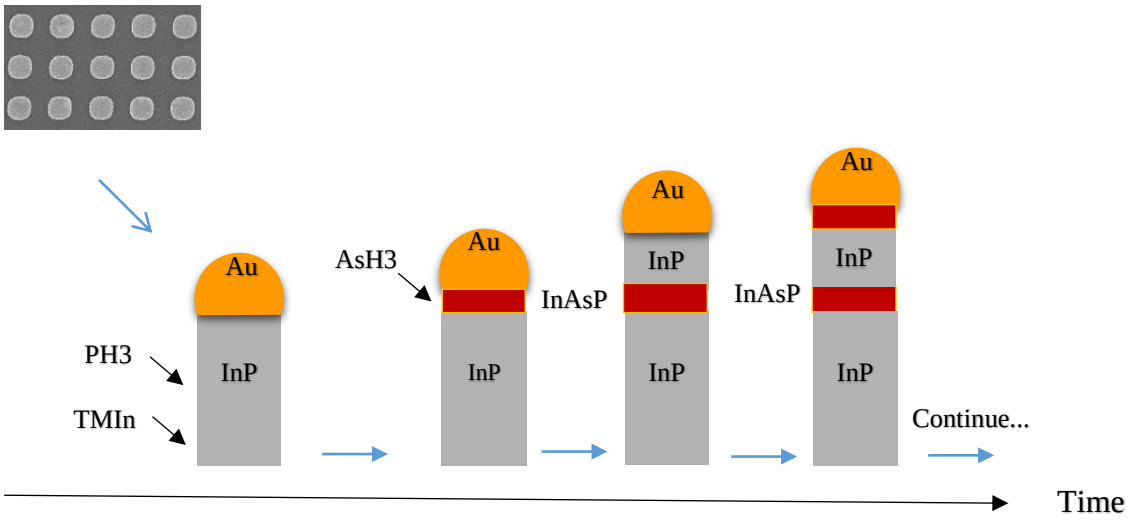

Figure 9: Schematic of the NW growth with the embedded QDiscs. For growing multiple QDiscs, the growth procedure is repeated

An SEM image of the grown array of vertically standing NWs on a substrate is shown in Fig. 10:

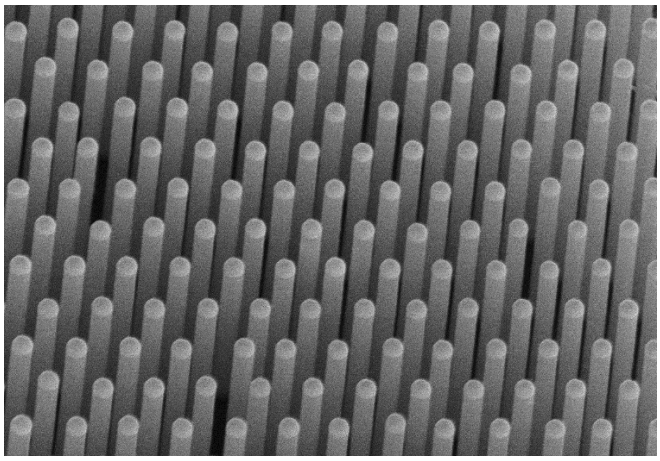

Figure 10: Tilted SEM image of as-grown NWs with axially embedded QDiscs. The Au NPs are visible at the top of the NWs

The grown QDiscs have a thickness of around 10 ± 1 nm, for a growth time of 2 seconds, 4-7 nm for a growth time of 1 second, as shown in the TEM images in Figs. 11 and 12. Energy dispersive X-ray spectroscopy (EDS) revealed a fairly sharp InAsP/InP [7] interface. Point measurements of the composition in the QDiscs yielded an As concentration between 60 to 80% for QDiscs grown for 2s, and around 55% for QDiscs grown for 1 s. The presence of P in the QDiscs can be attributed to the memory effect and diffusion during the growth process. As it can be seen from Fig. 11, the distances between QDiscs are different and they vary from 50nm at the base of the NW to 25nm near the NW tip. This reduction in InP barrier thickness is attributed to a decreased supply of In from the substrate [46].

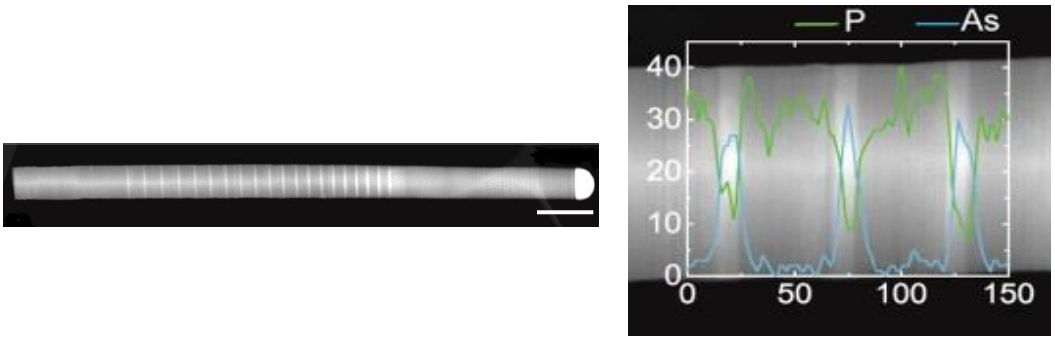

Figure 11: TEM image of an InP NW with 20 embedded InAsP QDiscs (left image). EDS line scan performed along the NW (right image). The green line represents P and the blue line shows the presence of As in the QDiscs. The scale bar is 200 nm [7]

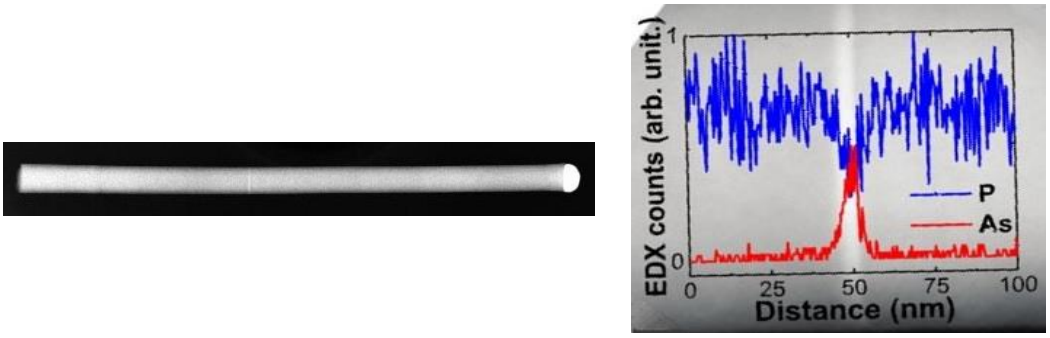

Figure 12: TEM image of an InP NW with a single InAsP QDisc (left image).EDS line scan performed along the NW (right image). The blue line represents P and the red line shows the presence of As in the QDisc [20]. Spatial resolution in EDS is 1.5nm.

3.1.2 Passivation

NWs are interesting candidates for novel optoelectronic devices like photodiodes and photodetectors. Besides their advantages, they also show some undesired features. One of their weaknesses is a high density of surface states due to the large surface to volume ratio. When there are surface states, more non-radiative recombination can happen which leads to shorter carrier lifetimes. Fortunately, InP NWs have fewer surface states and so lower surface recombination velocity than other III-V materials. Still, surface states on InP NWs lead to degradation of their optical and electrical properties [28]. To mitigate this problem, one can deposit an oxide layer to passivate the surface of the NWs. Among oxide films, a phosphorus oxide (PO_x) layer can improve the properties of InP NWs. Since PO_x is hygroscopic under ambient conditions, and so unstable, a capping layer of Al_2O_3 can be deposited. It is expected that the PO_x/Al_2O_3.passivation reduces the surface recombination and increases the carrier lifetime in luminescence events [24] [25] [44] [47] . Some studies [26] suggest that SiO_2 can also be an efficient layer for passivation. In order to confirm that, we made a comparative study of electro-optical properties of NW samples passivated by either a SiO_2 layer or a PO_x/Al_2O_3 layer.

3.1.3 Atomic Layer Deposition (ALD)

For producing a thin film on materials, some techniques are available and the one that is chosen in this work is ALD. ALD is a vapor phase method to deposit a thin layer of different materials on a surface. In this method, the surface of the substrate is exposed to alternating precursors introduced sequentially. ALD has shown significant advantages compared to other deposition techniques like chemical vapor deposition (CVD) since it has a better control over material thickness and composition. One of the ALD advantages is uniformity of the deposited layer on high-aspect ratio structures.

The choice of reactants (the materials to be deposited on the surface) that are suitable for ALD is limited. The reactant should be a volatile material to be in a gas phase at room temperature or higher temperature. Also, they should stay in the gas phase until they react with the sample surface, so they should not decompose before reaction. Hence, in order to have a high throughput process, the surface reaction should be quick and irreversible. The ideal reactant should easily cover all of the surface of the sample.

In a typical ALD process, first the reaction chamber is filled by the gaseous precursor and the precursor adsorbs on the sample surface. This is a self-limiting process, i.e., the precursor just adsorbs onto exposed surface areas and when all areas are covered, the adsorption stops. Then the other gas is introduced into the chamber and all steps are repeated. This sequence can be repeated until the desired thickness is achieved. During this process, a carrier gas like nitrogen is introduced into the chamber to remove side-products while the chamber is pumped out. The ALD process can be done in two ways: spatial ALD and temporal ALD. In the spatial ALD, the sample is moved between different positions and exposed to different precursors, but in the temporal ALD the sample is fixed in its position and different precursors are introduced

sequentially without overlap. The later method produces more conformal, uniform, symmetric and smooth thin film.

In this work, two different ALD machines are utilized to deposit two different oxide layers on the NW surface: ALD Savannah and ALD Fiji. The main process for the two ALD machines is similar and explained in the previous paragraph but there are some differences. The ALD Savannah has two operation modes called continuous mode and exposure mode. In the continuous mode, the N_2 carrier gas is flowing continuously while adding precursors or during pumping the chamber. In the exposure mode, one precursor is introduced first, and then the chamber is pumped out before the next exposure is run. The exposure mode provides a thin conformal film on high aspect ratio features, while the continuous mode facilitates fast and quick growth of thin conformal layers. The Fiji plasma ALD system has three operating modes: exposure mode for ultra-high aspect ratio structure, continuous mode for fast growth and plasma mode for growth of metals and nitrides.

In this project, we use two different passivation layers to investigate their effects on the optoelectronic performance of the NW/QDisc samples. Each sample is cleaved into three pieces. The first set is kept as-grown without any passivation. The second set is passivated with a POx/Al_2O_3layer using the ALD Fiji system and the last set is passivated by SiO_2 using the ALD Savanah setup. Deposition of POx/Al_2O_3 is done by a plasma-enhanced ALD system at room temperature. According to the Ref. [30], the temperature during the deposition has a significant effect on the quality of the passivation layer. For instance, deposition of POx/Al_2O_3 layers at elevated temperatures, 50-100 °C, leads to a decrease of the PL intensity compared to samples for which the deposition was carried out at room-temperature.

The SiO_2 deposition is carried out by the ALD Savannah system. The two precursors tris(tert-butoxy)silanol (TTBS) and trimethylaluminium (TMA) were used for adding Si and Al (acts as catalyst) to the chamber, respectively, in a self-limiting manner. The deposited layers are thus expected to be SiO_2 with some in-mixing of Al. For producing thicker layers, the ALD is operated in the exposure mode. In this operation mode, the precursors have sufficient time to diffuse over the sample surface, which leads to producing a uniform layer. Then an extra layer of Al_2O_3 is deposited, which acts as an adhesive layer, since a resist that is used in processing step for device fabrication cannot stick to the SiO_2 layer well and it causes undesired oxide etching in further steps.

The passivation increases the NW diameter to 20 nm for the POx/Al_2O_3 layer and 90 nm for the SiO_2 layer comparing to the as-grown NWs. The SEM images of the NWs are shown in the Figs. 13 and 14 below:

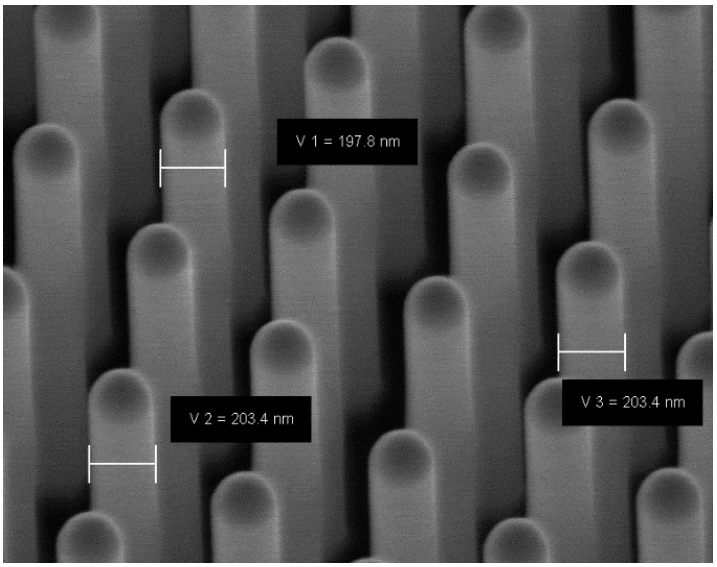

Figure 13: NWs passivated with a POx/Al_2O_3 layer

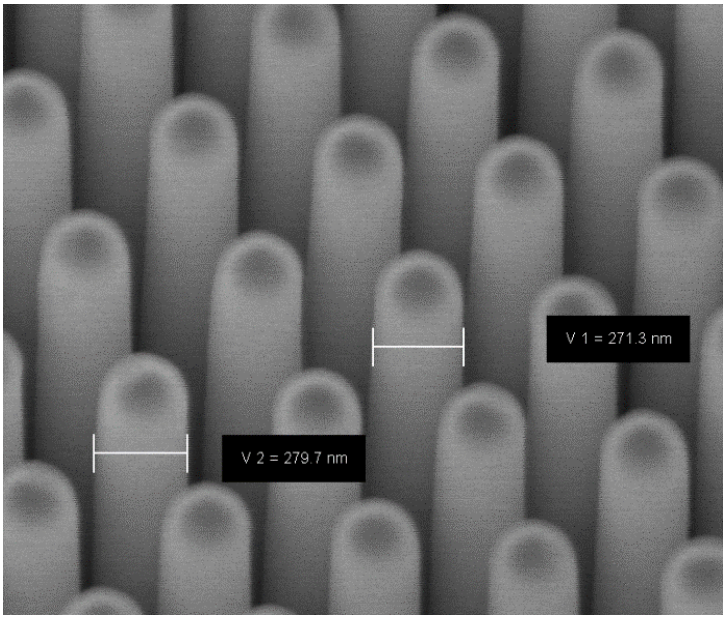

Figure 14: NWs passivated with a SiO_2 layer.

4 Characterization techniques

In this work, two main methods were used to characterize the effect of passivation of the NWs. The optical properties were probed by photoluminescence, while the electrical properties were investigated by an in-situ electrical nanoprobe technique as described below.

4.1 Photoluminescence (PL) spectroscopy

When a semiconductor is excited by photons with higher energy than the bandgap, electrons can be excited from the valence band (VB) to the conduction band (CB), leaving behind a hole in the VB. This process is called interband absorption. This configuration is however unstable. After a very short time, of the order of picoseconds, the charge carriers thermalize to the bottom of the respective band edge and subsequently recombine with a hole on a time scale of hundreds of picoseconds to nanoseconds. In this recombination process, photons with energy of about the bandgap are emitted. Figure 15 shows a schematic of the optical generation and recombination processes. In photoluminescence (PL), the energy distribution of these emitted photons is measured while exciting the semiconductor with a laser. PL spectroscopy provides information about e.g. band gap, band offsets, confinement and presence of impurity states.

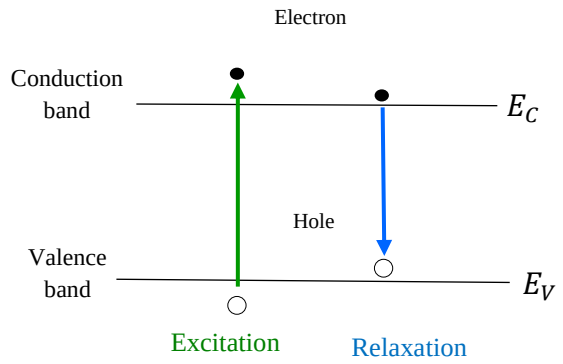

Figure 15: Schematic of interband transitions in a semiconductor leading to generation (green arrow) and recombination (blue arrow) of charge carriers.

The discussion above is however somewhat simplified. In fact, there are two types of semiconductors with respect to their bandgap: direct bandgap and indirect bandgap semiconductors. If the minimum of the CB and maximum of the VB have the same momentum value (k) in the reciprocal space (k-space), then the semiconductor has direct band gap. In a direct bandgap semiconductor, the recombination of an electron with a hole leads to the emission of a photon with energy roughly equal to the bandgap energy due to the energy conservation rule. InP is one example of a direct bandgap semiconductor. In contrast, the CB minimum and VB maximum are at different k for indirect bandgap materials e.g. Si. In this case, the recombination of an electron with a hole requires the emission of both a phonon (lattice

vibration) to conserve momentum, and a photon to conserve energy (Fig. 16). Fewer photons will be emitted compared to a direct bandgap material, and the photons will have an energy smaller than the bandgap by an amount corresponding to the phonon energy.

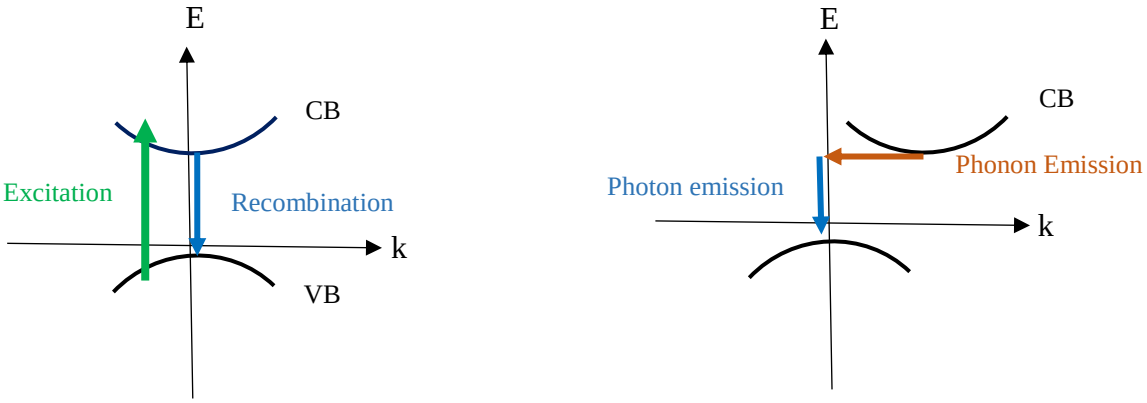

Figure 16: Direct bandgap semiconductor (left panel). The minimum of the CB and maximum of the VB have equal momentum. The electron-hole recombination process leads to the emission of photons with an energy equal to the bandgap. Indirect bandgap semiconductor (right panel). The red and blue arrows show the emission of a phonon and photon, respectively.

Photoluminescence emission can originate from band-to-band recombination or from recombination processes involving defects and interfaces. It was reported that if InP NWs were excited by low energy photons, the emission energy was close to the ZB bandgap indicating band-to-band recombination in ZB segments. If the excitation energy was gradually increased the emission energy shifted toward the WZ bandgap, indicating a band-to-band recombination process taking place in WZ segments [48]. Another feature of WZ InP is splitting of the valence band [40] and the energy difference between the two valence bands is about 40 meV. From this, it can be inferred that the PL emission can originate from ZB segments or from WZ segments (either the first or the second valence band). Another recombination process involves spatially indirect transitions as shown in Fig. 17 below.

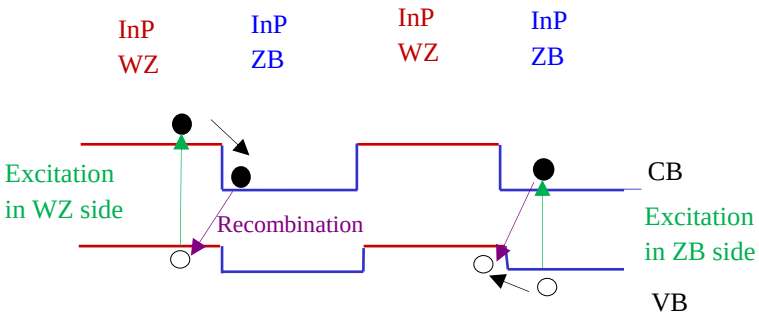

Figure 17: Formation of type-II band alignment in InP ZB/WZ heterostructures. The purple arrows show possible spatially indirect PL emission transitions. The green arrows show interband excitations of the ZB and WZ segments, respectively. The black arrows also show the relaxation of an electron and a hole to lower states.

After an electron is excited from the VB to the CB in the WZ (ZB) segment, the electron (hole) relax to lower states in the CB of the ZB (VB of the WZ) segment, or at the defect states not shown in Fig. 17.

4.2 Experimental PL set-up

Figure 18 shows the schematic of the PL set-up which is used for this project. In this experiment, a green laser with wavelength 532nm and power 2 W/cm^2 is used as the excitation source. To facilitate power-dependent PL measurements, a filter wheel with different attenuation is mounted in the laser path. The laser beam goes through a beam splitter and then it is focused on the sample by an objective lens. The sample is placed in a cryostat which is fixed on a XY-stage to enable low-temperature PL measurement on a single selected NW. The luminescence from the NW sample is collected by the same objective lens, split by a beam splitter and then focused onto the entrance slit of the spectrograph with a focusing lens.

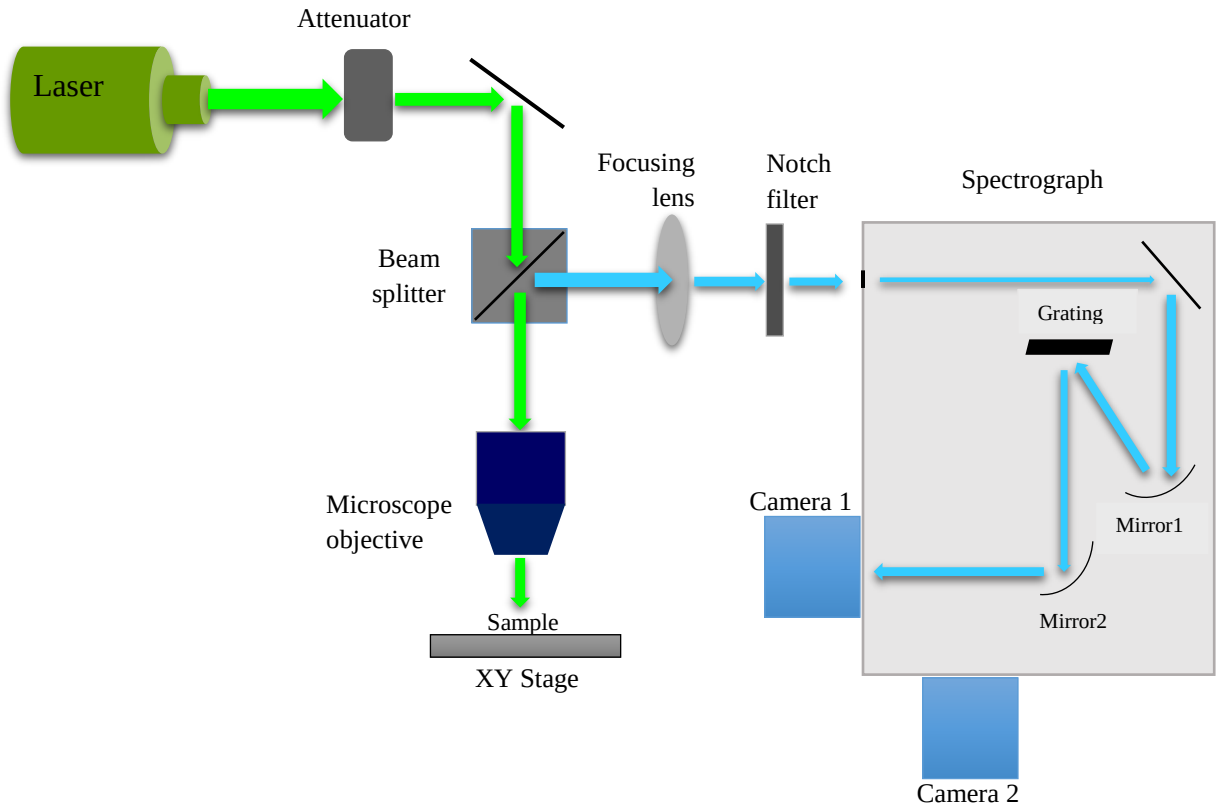

Figure 18: Schematic of a PL set-up

To block the laser light from entering the spectrograph, a notch filter is mounted before the entrance slit. Inside the spectrograph, the collected PL light is collimated by a mirror 1 and then dispersed by a grating. By use of a focusing mirror 2, the PL spectra can be focused on a detector. Two detectors (cameras) are used in these measurements. One of the cameras is used for focusing the laser spot on the selected NW. The other camera is an InGaAs array detector

which provides and detects the PL spectra from the sample. A computer with installed LabView software is used to control the monochromator and cameras.

4.3 Nanoprobe-enabled single nanowire measurements

Electrical characterization of single NWs typically requires challenging and time-consuming lithographic techniques to make electrical contacts to the NW. For this, NWs are removed from the substrate and transferred onto another insulating substrate. After that the substrate is patterned by electron beam lithography (EBL), followed by a metal deposition step to make the contacts. In contrast, a sharp nanoprobe, placed inside of an SEM, can be used for characterization of vertically standing NWs on a substrate without any need of transferring. Our nanoprobe system from Kleindiek Nanotechnik is mounted inside of a Hitachi SU8010 SEM (Fig. 19). The position of the sample is controlled by a piezoelectric positioning stage. A tungsten (W) nanoprobe is gently pressed into the Au seed particle at the tip of a selected NW. The substrate forms a grounded back contact. By applying a bias to the nanoprobe, sets of I-V characteristics can conveniently be recorded [49].

Moreover, when the contacted NW is exposed to the electron beam inside the SEM, electron-hole pairs are generated. If this generation takes place in the depletion region of a p-n junction, or within a diffusion length, the electron-hole pairs are separated by the electric field forming a current in the external circuit. This mechanism is similar to generation of a photocurrent in a solar cell or photodetector.

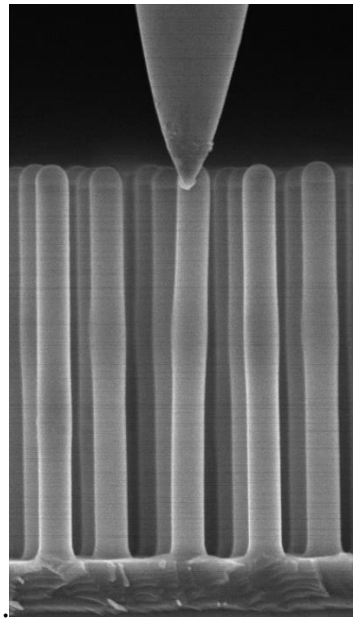

Figure 19: SEM image of a contacted NW in one of the investigated samples in this study. The W nanoprobe, pressed into the Au particle, is seen in the top part of the image. The bending of the NW is a good sign of the formation of a reliable contact between nanoprobe and NW.

In this work, the current is collected in dark and under electron beam irradiation. The obtained I-V curve under irradiation provides a reasonable idea of how the samples would behave under illumination with light while there can still be fundamental differences.

It should be noted that nanoprobe characterization of NWs as described above can suffer from a parasitic metal-semiconductor (Schottky) junction formed between the Au seed particle and NW [50]. In our case, however, the top segment of the NW is $n^+ - InP$, which prevents the formation of a Schottky junction.

5 Results and Discussion

The following three sets of samples, comprising n^+-i-n^+ InP NWs grown on p^+-InP substrates, are examined during this project:

- 12648: InP NWs with a single QDisc, the growth time for the QDisc is 2 second.
- 12649: InP NWs with 20 QDiscs, the growth time for the QDiscs is 2 seconds
- 12650: InP NWs with 20 QDiscs, the growth time for the QDiscs is 1 second

Each set has three different samples denoted “a”, “b” and “c”, indicating as-grown NWs, NWs passivated with POx/Al_2O_3 and NWs passivated with SiO_2, respectively. For example, sample 12648a comprises as-grown NWs with a single QDisc, 12649b comprises POx/Al_2O_3-passivated NWs with 20 QDiscs grown for 2 seconds.

5.1 PL results

We first did PL measurements on as-grown NW arrays at 4K. These PL data are not very useful, since the signal is dominated by the PL emission from the substrate.

In the next step, we carried out PL measurements on single NWs which were mechanically transferred from the growth substrate onto a gold-coated Si/SiO_2, substrate (See Fig. 20).

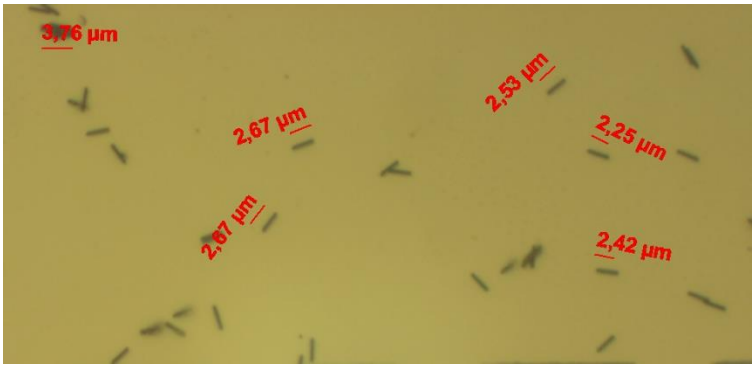

Figure 20: Optical microscope image of NWs lying on a substrate. Single NWs, as well as bunches of NWs are clearly visible

5.1.1 Sample 12648

Power-dependent PL measurements were done on single NWs. Figure 21 below shows logarithmic plots of the PL intensity vs photon energy.

12648a

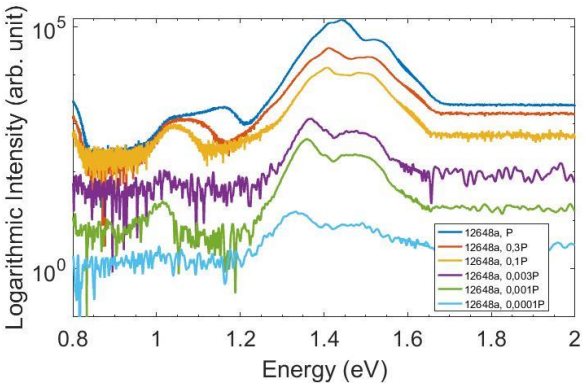

12648b

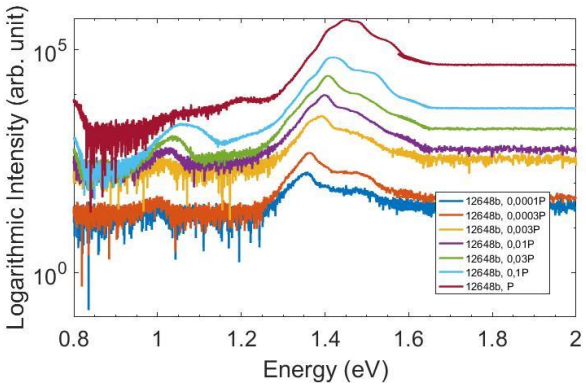

12648c

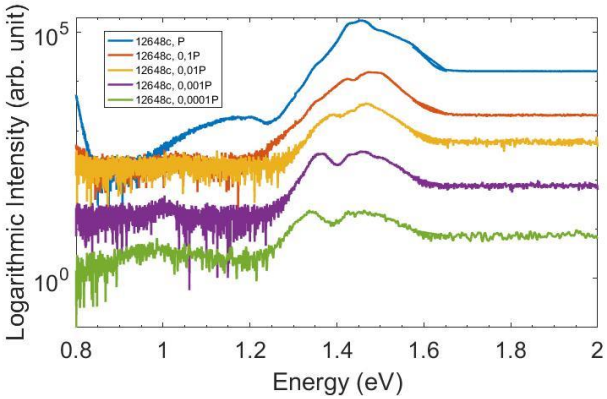

Figure 21: Power-dependent PL on single NWs with a single embedded QDisc. 12648a is an as-grown NW, 12648b is a POx/Al_2O_3-passivated NW while sample 12648c is a NW passivated with SiO_2. The legends show the applied power intensities. The upper trace corresponds to the PL spectra taken at full power $P=2W/cm^2$.

As seen, the InP peak is clearly more prominent than the InAsP QDisc peak. We can see both WZ and ZB InP peaks for all three samples, but the intensities are different. The PL peak reflecting the QDiscs is generally shifted to higher energy compared to a previous study on similar samples [20] [46] showing a QDisc-related signal at around 0.85-0.95 eV. The difference can be attributed to different QDisc composition or thickness. The QDisc peak positions, for as-grown NWs, are in reasonable agreement with the expected interband transition energy estimated from calculations presented in the Appendix. We considered three different quantum wells with thicknesses a=4, 7 and 10 nm, respectively. These thicknesses were selected because the grown QDiscs have a thickness of around 10 ± 1 nm, for a growth time of 2 sand 4-7 nm for a growth time of 1 s.

Moreover, the QDisc peak shifts to higher energy with increasing excitation power which is due to state filling. Another feature is that the emission spectra are quite broad for all sets of the samples. This broadening can be related to the Coulomb interaction between excitons (bound electron-hole pairs) and distributed surface charges on the NWs [26].

For understanding the effects of the passivation, we compare the PL peak intensities from the InP NW and InAsP QDiscs, averaged over typically 5-6 NWs from each sample set. In order to make a fair comparison, we use box plots. Figure 22 gives a simple explanation of the interpretation of such plots. The boxes include the 25th and 75th PL intensity percentiles which mean that 25% and 75%, respectively, of the observed PL intensities are below the corresponding percentiles. The boxes also include the average and median, but the average value is more important for comparison than the median.

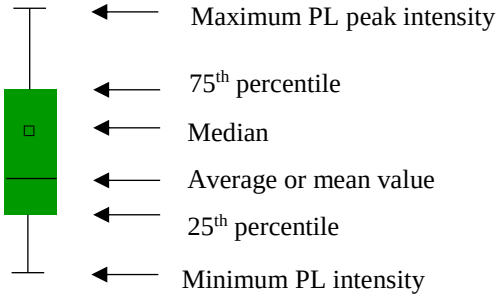

Figure 22: Simple explanation of the box plot

The comparison of the PL intensities for different NWs is uncertain since the excitation and collection of the PL might vary from NW to NW, even though the alignment and focusing are done carefully.

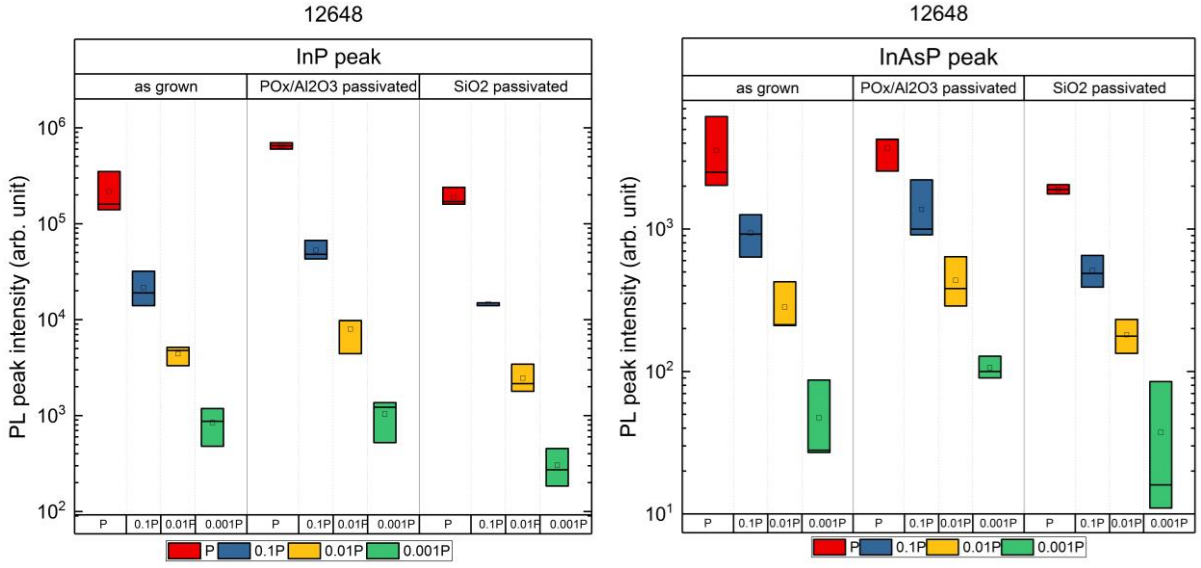

Figure 23: PL peak intensities for InP (left panel) and InAsP (right panel) taken at four different powers (full power P is shown in red box, 0.1P in blue box, 0.01P in yellow box and 0.001P in green box) for as-grown and passivated NWs to compare the effect of the passivation. The height of the boxes indicates the spread in PL intensities between different NWs. The solid black line in each box indicates the corresponding average PL intensities for the investigated set of NWs.

Several (5-6) single NWs from each sample are investigated. In Fig. 23, the height of the boxes corresponds to the spread in all PL peak maximums for the set of NWs and the important

parameter is the average shown by the solid black line inside the boxes. Each color box indicates a fixed power at which the PL spectra were collected. Each panel (left or right) has three different vertical sub-sections which correspond to PL intensities for as-grown NWs PO_x/Al_2O_3-passivated NWs and SiO_2-passivated NWs.

For all powers, the average peak intensity of the NWs passivated with PO_x/Al_2O_3 is higher compared to the as-grown NWs, except possibly for the InAsP peak at full power where the passivation makes no significant difference. Also, we can see that SiO_2 passivation has an undesired effect, decreasing the PL intensity compared to the as-grown NWs.

The dependence of the PL peak positions on the passivation could also be investigated more in detail. Figure 24 shows the PL peaks for as-grown and passivated NWs. The main plot and inset show the PL signals related to InP and InAsP QDiscs, respectively.

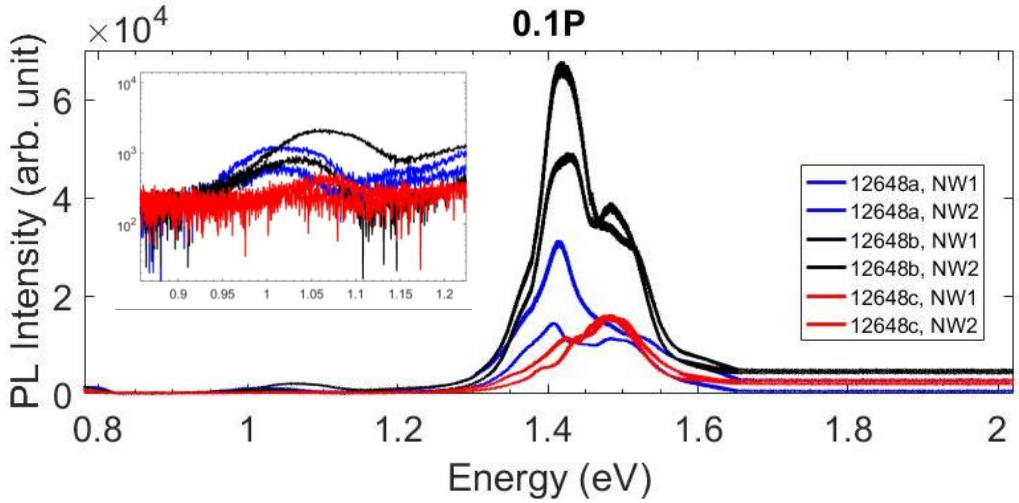

Figure 24: PL peaks for samples 12648 with a single embedded QDisc. The main panel shows data recorded at the excitation power 0.1P. Six NWs were measured: two of them are as-grown NWs, 12648a (blue curves), two are passivated with PO_x/Al_2O_3, 12648b (black curves) and two are passivated with SiO_2, 12648c (red curves). The inset shows the corresponding PL spectra of the InAsP QDiscs.

For this sample, all NWs exhibited a weak PL from the QDiscs, so we are not able to compare them properly. However, we can say that there is a blue shift after passivation with both PO_x/Al_2O_3 and SiO_2. Interestingly, the ZB InP peak is more prominent than the WZ InP peak for the as-grown and PO_x/Al_2O_3-passivated NWs, in contrast to the SiO_2-passivated NWs which show the opposite trend.

5.1.2 Sample 12649

For the sample 12649 with 20 QDiscs (grown for 2 s), we are unfortunately not able to make any optical comparisons since one of the samples was destroyed during the experiment.

5.1.3 Sample 12650

Here we consider the NWs with 20 thinner QDiscs (grown for 1 second).

12650a

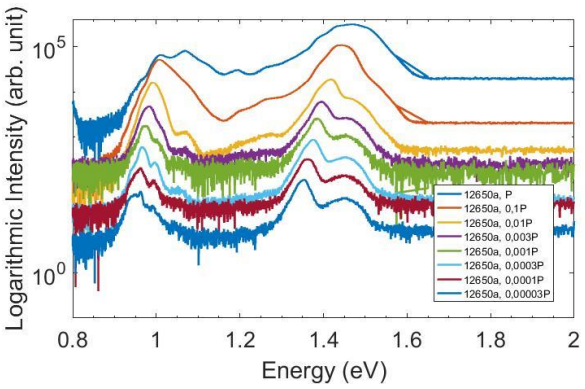

12650b

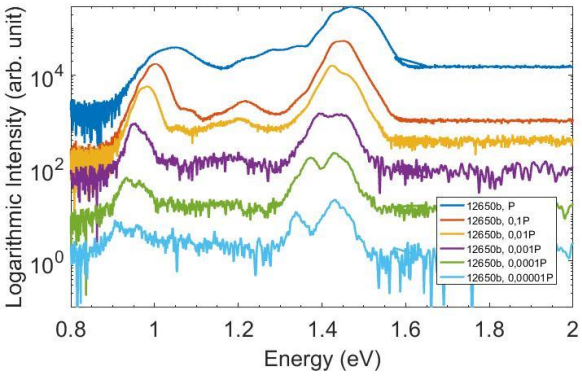

12650c

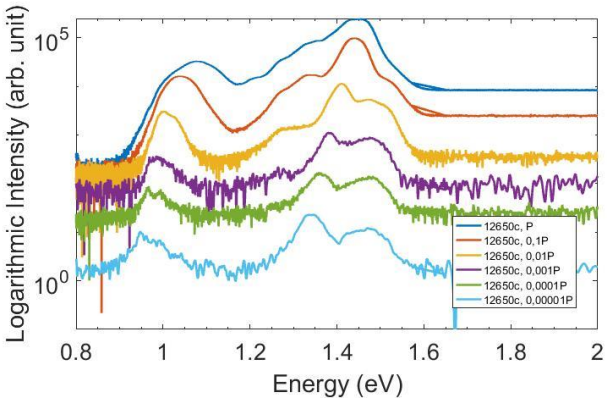

Figure 25: Power-dependent PL on single NWs with 20 embedded QDiscs. 12650a is an as-grown NW, 12650b is a POx/Al_2O_3-passivated NW and the sample 12650c is a NW passivated with SiO_2. The legends show the applied power intensities. The upper trace corresponds to the PL spectra taken at full power $P=2W/cm^2$.

For this sample, the PL intensities from all QDiscs are significantly higher compared to the single QDisc sample (12648) and almost comparable to the InP peaks. The QDiscs peaks broaden and shift towards higher energies when the power is increased, which is related to the state filling effect. The WZ and ZB InP peaks are both visible at lower excitation power but seem to merge and blue-shift at higher excitation power, where the ZB peak shows blue shift with increasing the power intensity.

For investigating the effect of the passivation, we show again a box plot in Fig.26 (similar to Fig.23).The PL intensity from the InP is again improved by passivation with PO_x/Al_2O_3,while it decreases after SiO_2 passivation. Interestingly, an opposite trend is observed for the QDiscs peaks. The passivated NWs exhibit weaker QDiscs PL intensity compared to the as-grown NWs. It can be related to the different passivation materials, i.e., SiO_2 and PO_x/Al_2O_3can be

proper passivation layers for InP but they are not able to passivate the InAsP discs in a desired way.

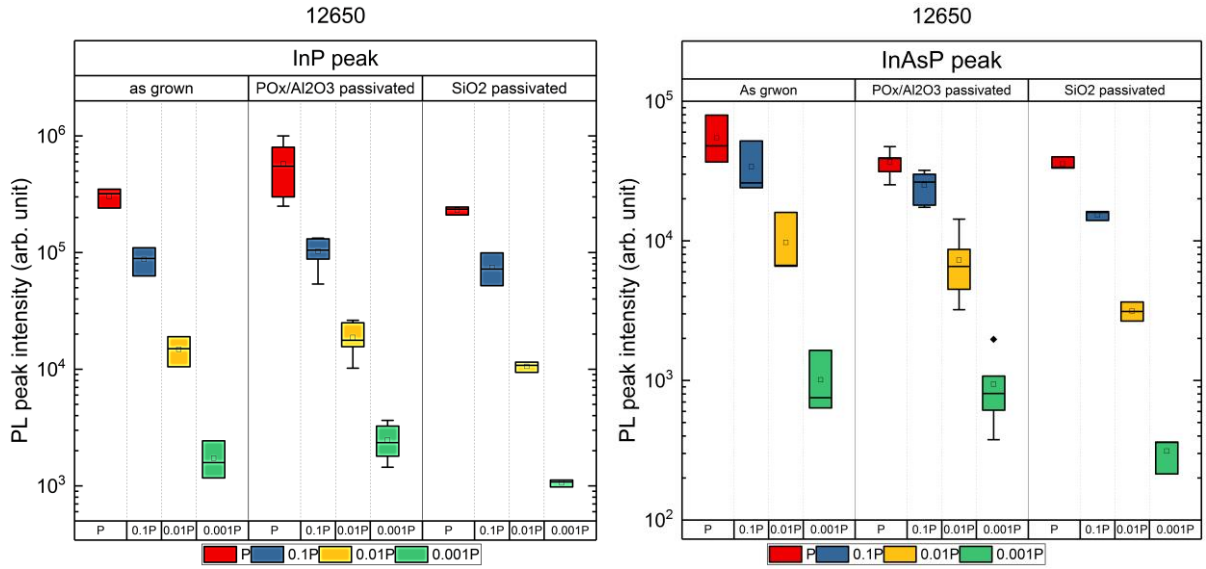

Figure 26:PL peak intensities for InP (left panel) and 20 InAsP QDiscs (right panel) taken at four different powers (full power P is shown in red box, 0.1P in blue box, 0.01P in yellow box and 0.001P in green box) for as-grown and passivated NWs to compare the effect of the passivation. The height of the boxes indicates the spread in PL intensities between different NWs. The solid black line in each box indicates the corresponding average PL intensities for the investigated set of NWs.

For this sample, due to the increased numbers of QDiscs, we can clearly observe the PL from the QDiscs and we are able to compare samples with different passivation (Fig. 27).

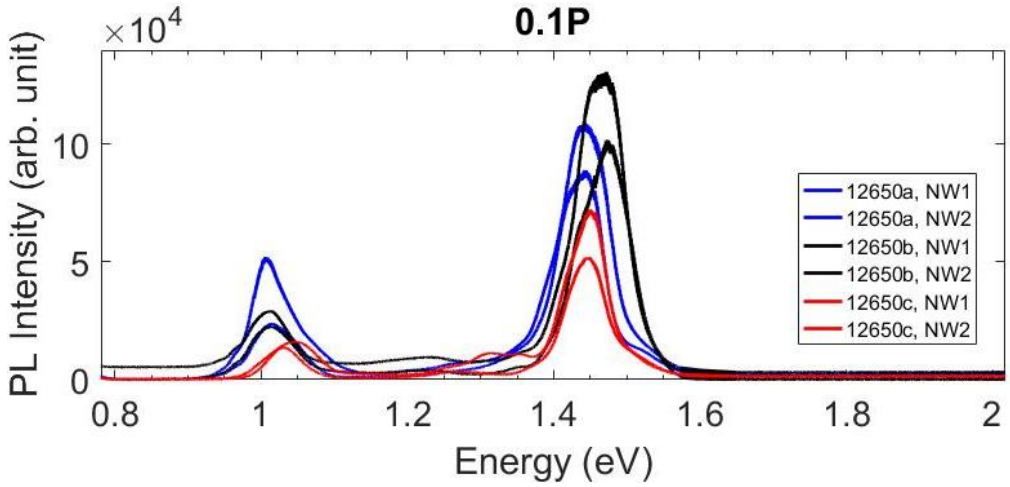

Figure 27: PL peaks for samples 12650 with 20 embedded QDiscs. The main panel shows data recorded at the excitation power 0.1P. Six NWs were measured: two of them are as-grown NWs, 12650a (blue curves), two are passivated with PO_x/Al_2O_3, 12650b (black curves) and two are passivated with SiO_2, 12650c (red curves).

For the InP peak, this plot not only confirms the previous observation regarding the PL peak enhancement by the PO_x/Al_2O_3 passivation, but also shows a small blue shift in peak position

for the PO_x/Al_2O_3-passivated NWs, compared to as-grown and SiO_2-passivated NWs. For the InAsP QDisc peak, the passivation does not have a significant effect on the PL intensity while the as-grown NWs exhibit higher PL intensity than passivated NWs. It was expected that the QDisc peaks should shift to higher energies compared to the samples with thicker QDiscs (grown for 2 s), due to the increased quantum confinement (based on the calculations in the Appendix), but no clear trend was observed.

To summarize, the PO_x/Al_2O_3 passivation enhances the PL intensities for the InP NWs but neither PO_x/Al_2O_3 nor SiO_2 shows any significant intensity enhancement for the InAsP QDiscs.

5.2 Nanoprobe characterization

In order to investigate the effects of passivation on the electronic behavior of the NWs, nanoprobe-enabled IV measurements were carried out. To do so, NW samples were mounted on the sample holder of an in-situ nanoprobe setup installed in an SEM (Hitachi) setup. The W nanoprobe, plunged into the Au seed particle at the top of a vertically standing NW, served as one electrode while the substrate was used as back contact.

5.2.1 Sample 12648

Nanoprobe-enabled (I-V) results for all single QDisc-in-NW samples are shown in Fig. 28. We studied 4 NWs in each sample, so the different colors in the plots correspond to separate NWs. It can be seen that there is an induced current, as well as a voltage-shift around 0V, under illumination by the electron beam. This observation is in agreement with the effect of light on a photodiode or solar cell.

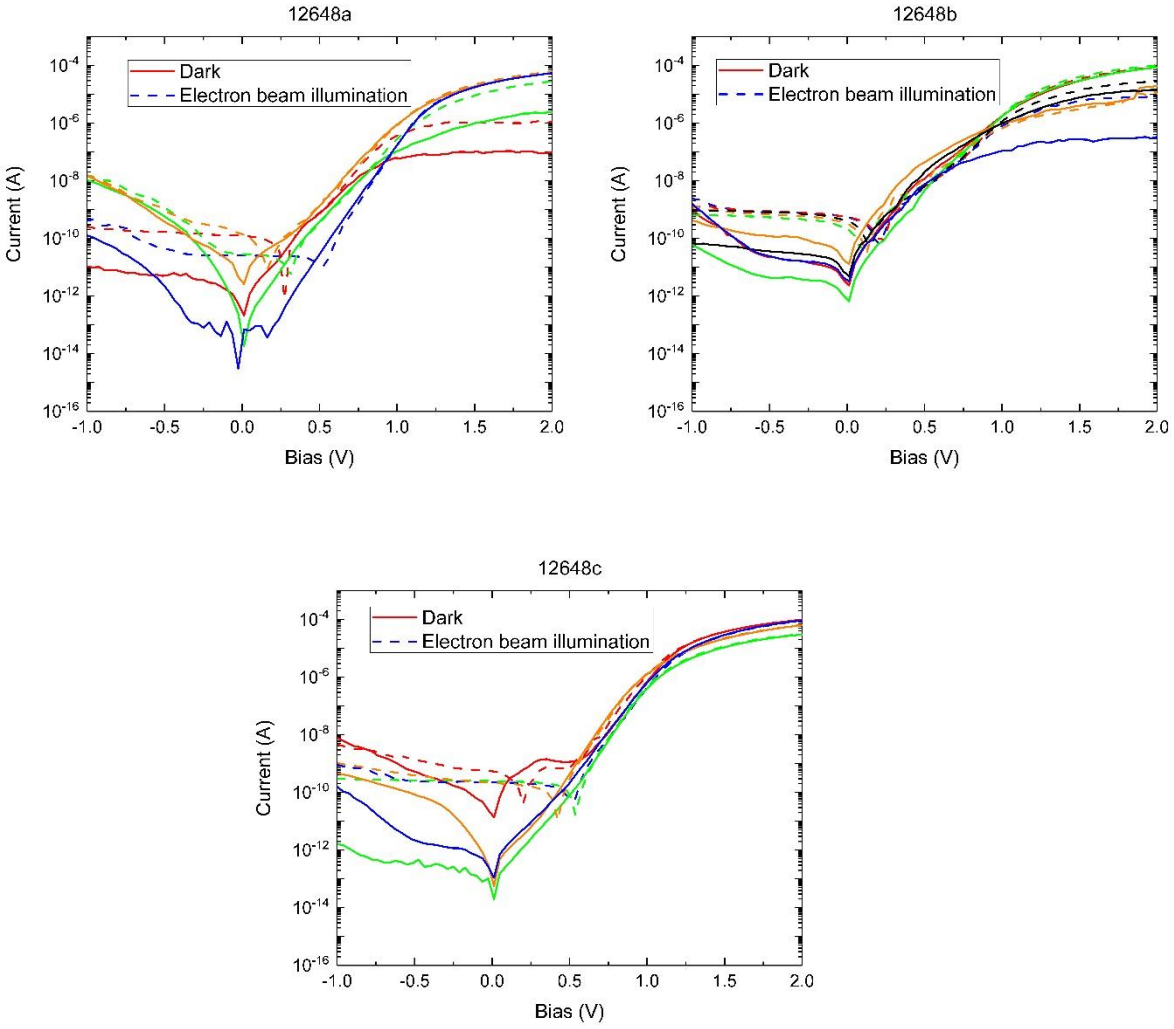

Figure 28: I-V characteristics of as-grown NWs (12648a), NWs passivated with PO_x/Al_2O_3 (12648b) and NWs passivated with SiO_2 (12648c). The NWs for these samples contain a single QDisc. The solid curves represent I-V data in dark while the dashed curves are I-V data under electron beam illumination.

According to the plots, all three samples demonstrate a diode-like I-V behavior which is due to p-n junction between the p-substrate and bottom n-segment of the NWs. Also, since the nominal intrinsic region is slightly p-doped by Zn to compensate for the unintentional n-doping, a formation of a junction between this region and adjacent n-doped regions is possible.

In order to evaluate the effect of different passivation layers, we extract an average value of the dark currents at -1V and 2V for all NWs in each sample and plot them in Fig. 29(a). Evidently, the average current for the as-grown NWs (12648a) at -1V is about one order of magnitude higher than for the two passivated samples. . However, the mean value of the leakage current is reduced about one order of magnitude for the PO_x/Al_2O_3 and SiO_2 passivated NWs compared to the as grown NWs. The reduction in leakage current indicates the effectiveness of the passivation layer by suppressing the effect of surface states. This is also supported by higher

forward current for the passivated NWs in comparison to the as-grown NWs. The estimated rectification ratio (the ratio of the forward current to the leakage current) for different samples are shown in Fig. 29(b). As seen, the average value of the rectification is at least one order of magnitude higher for the passivated NWs compared to the as-grown NW. Slightly better electronic performance of NWs passivated with SiO_2 is in contrast to the PL data where PO_x/Al_2O_3 NWs demonstrated higher PL intensity.

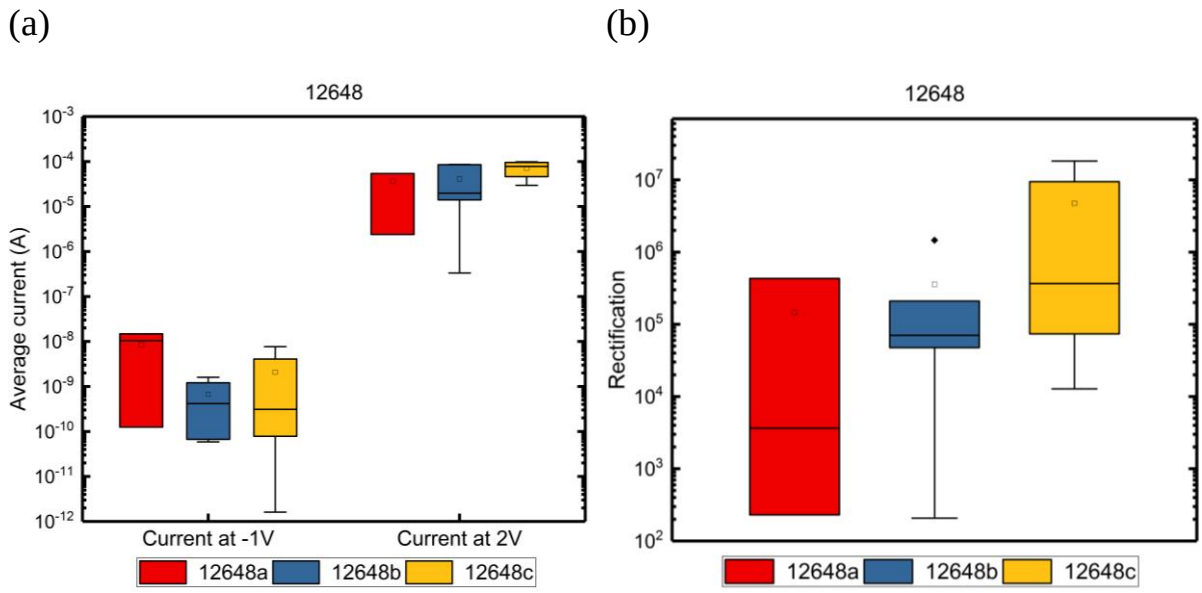

Figure 29:(a) Average currents taken at -1V and 2V for as-grown NWs (12648a, red boxes), NWs passivated with PO_x/Al_2O_3.(12648b, blue boxes) and NWs passivated with SiO_2(12648c, yellow boxes).(b) Ratio of forward current to leakage current (rectification) at -1V and 2V (data taken from (a)).

5.2.2 Sample 12649

I-V behaviors of the sample 12649 (20 QDiscs in a NW) are also characterized by the nanoprobe setup and results are shown in Fig. 30.

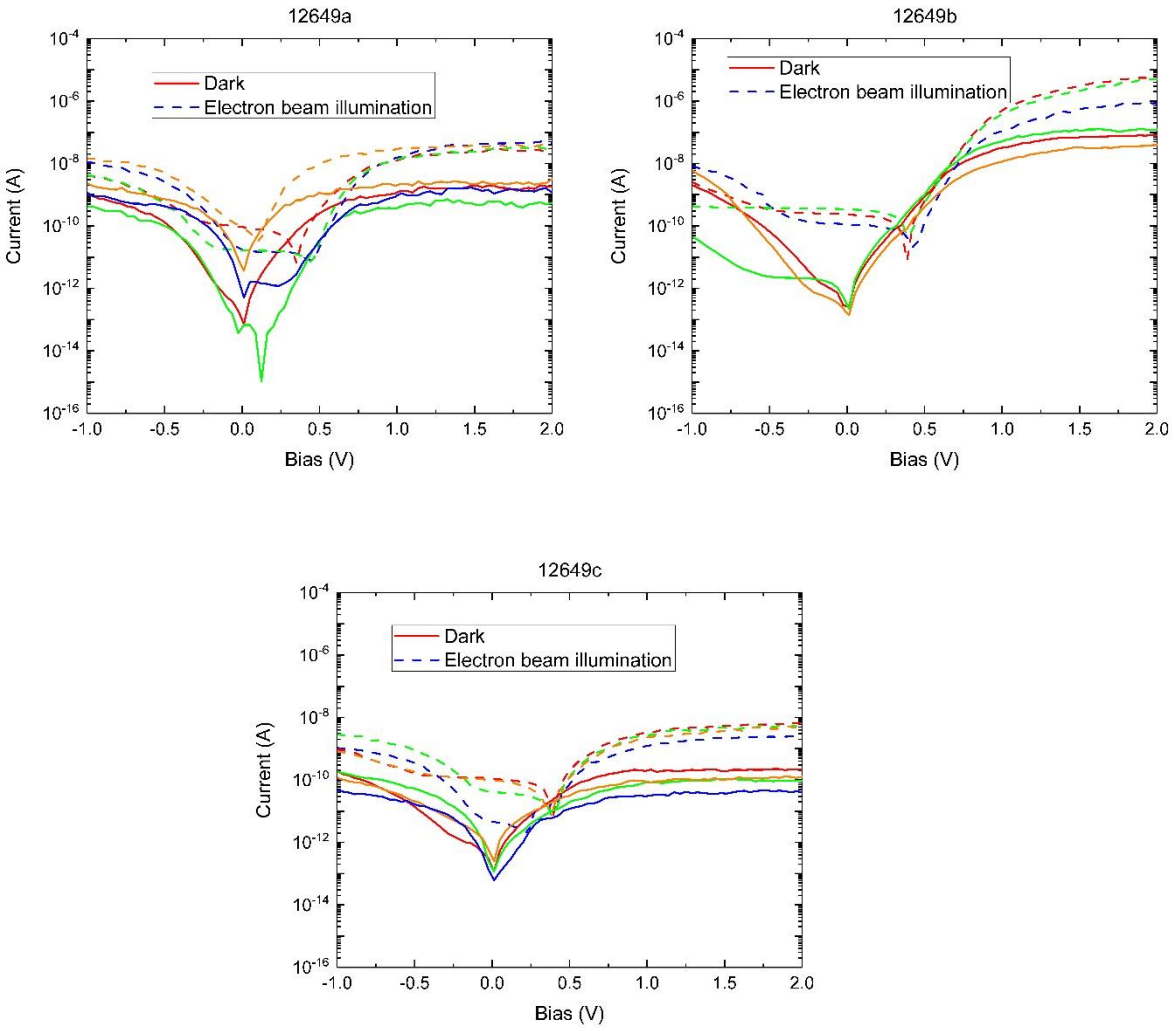

Figure 30: I-V characteristics of as-grown NWs (12649a), NWs passivated with PO_x/Al_2O_3 (12649b) and NWs passivated with SiO_2 (12649c). Each NW comprises 20 QDiscs. The solid curves represent I-V data in dark while the dashed curves are I-V data under electron beam illumination

Since these samples comprise 20 QDiscs with varying thickness (9-12 nm) and compositions (P concentration is varied from 20% to 80%), the interpretation of the I-V data might be more challenging. A comparison of the I-V of the sample 12649a with 12648a (both as-grown NWs), one can notice that the current level under forward bias is smaller for NWs with 20 QDiscs, which can be attributed to trapping of the carriers by QDiscs. Moreover, the as-grown sample, 12649a, demonstrates very low rectification less than a factor of 10, as shown in Fig. 31(a). As seen from the extracted leakage current and rectification values shown in Fig. 31 (a) and (b), the ALD passivation using PO_x/Al_2O_3 can effectively enhance both the leakage current and the rectification behavior. According to Fig. 31, the average value of the rectification for the PO_x/Al_2O_3-passivated sample is one order of magnitude higher than for as-grown NWs and SiO_2-passivated.NWs. This confirms an effective passivation of InP/InAsP NW heterostructures by ALD of PO_x/Al_2O_3.

Also, if the leakage current for this sample and previous sample with a single embedded QDisc in each NW is compared, we can see a higher leakage current in sample 12649, which can be due to electron tunneling through the barriers and through the depletion regions.

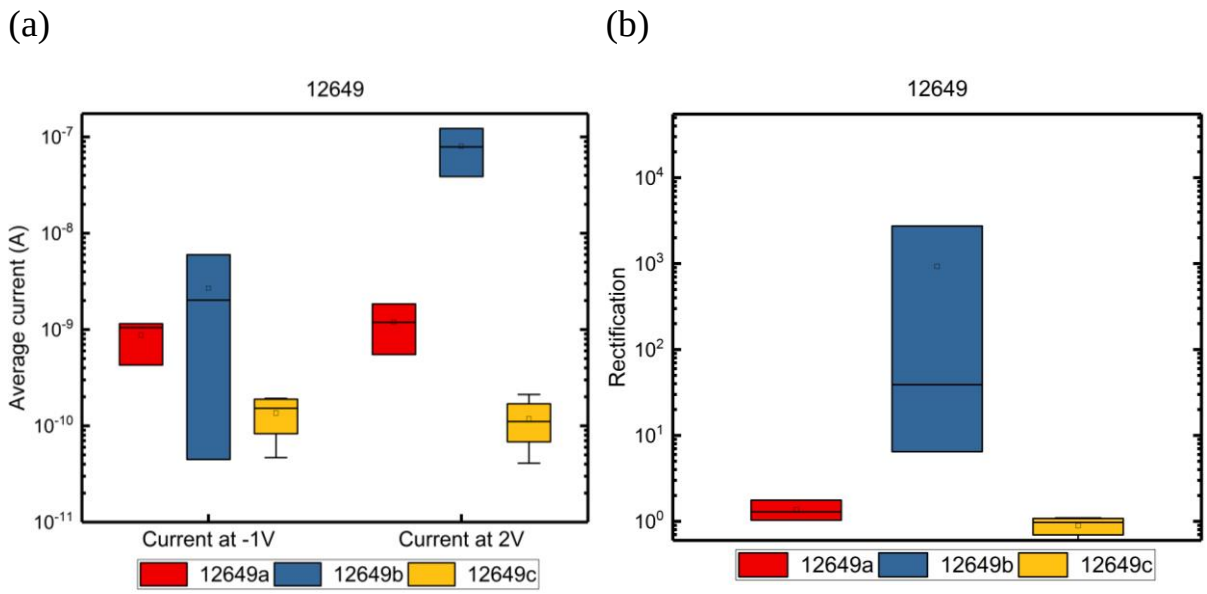

Figure 31: (a) Average currents taken at -1V and 2V for as-grown NWs (12649a, red boxes), NWs passivated with PO_x/Al_2O_3(12649b, blue boxes) and NWs passivated with SiO_2 (12649c, yellow boxes) to see the effect of passivation on the leakage current (b) Ratio of forward current to leakage current (rectification) at 2V bias (data taken from (a)).

5.2.3 Sample 12650

In order to further analyze the effect of passivation on InP/InAsP NW heterostructures, we perform nanoprobe-enabled I-V measurements on 20 thinner QDiscs-in-NW samples, where the growth time for the QDiscs was set to 1s. The measured I-V data for all three samples are shown in Fig. 32.

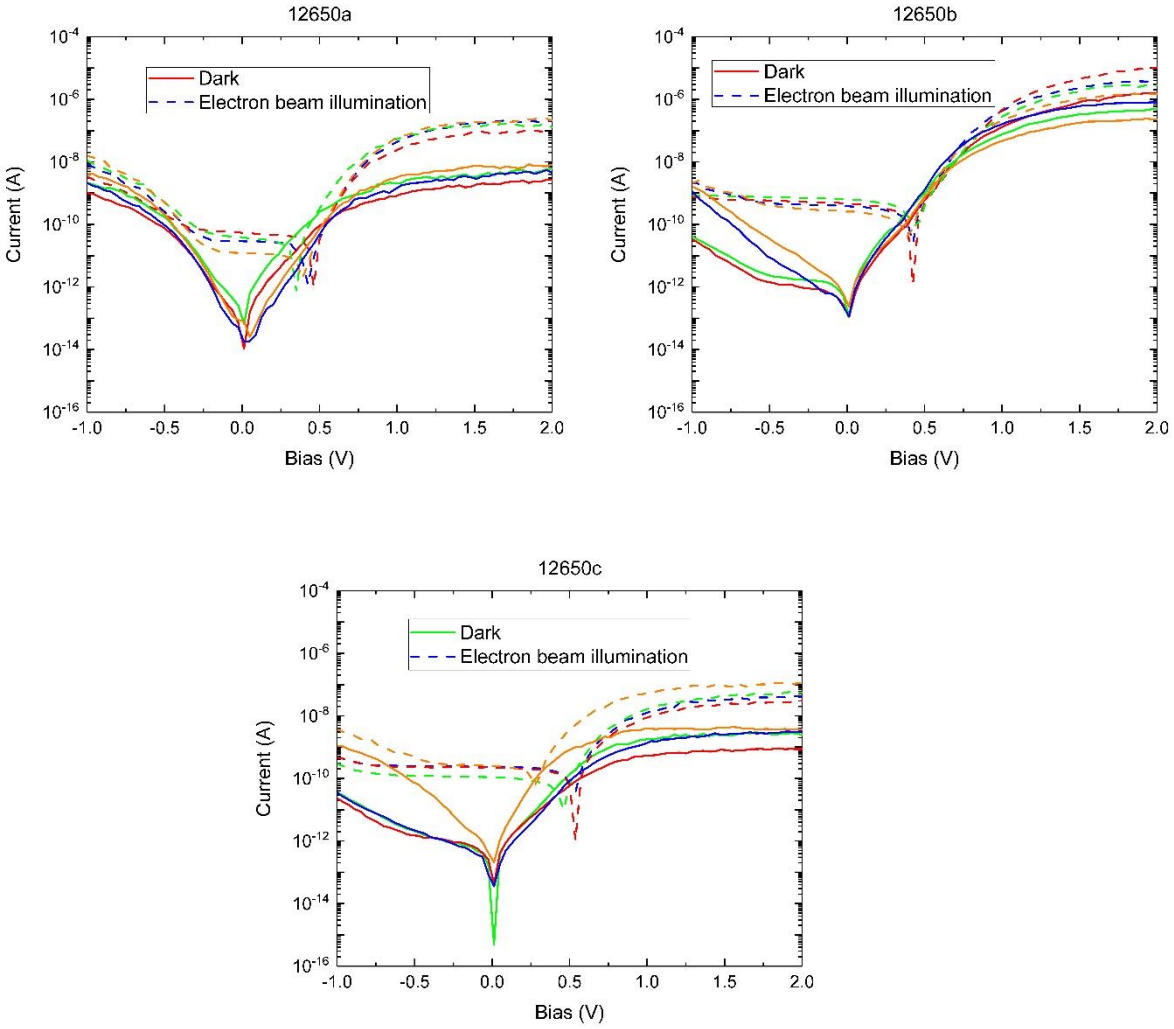

Figure 32 : I-V characteristics of the as-grown NWs (12650a), NWs passivated with PO_x/Al_2O_3 (12650b) and NWs passivated with SiO_2 (12650c). Each NW comprises 20 thin QDiscs. The solid curves represent I-V data in dark, while the dashed curves are I-V data under electron beam illumination.

Similar to the sample 12649, these NWs demonstrate a poor I-V behavior when as-grown, which confirms the deteriorating effect of the surface states. However, by ALD passivation of PO_x/Al_2O_3, the leakage current reduces by about two orders of magnitude compared to the as-grown NWs and the forward current enhances similarly. The resulting rectification, shown in Fig. 33b, is consequently of the order of 10000, which is substantially better than as-grown NWs and NWs passivated with SiO_2. It is clear that ALD of SiO_2 doesn't improve the electronic

performance of the InP/InAsP NW heterostructures. This might be due to a poor passivation effect of SiO_2 on the InAsP segment.

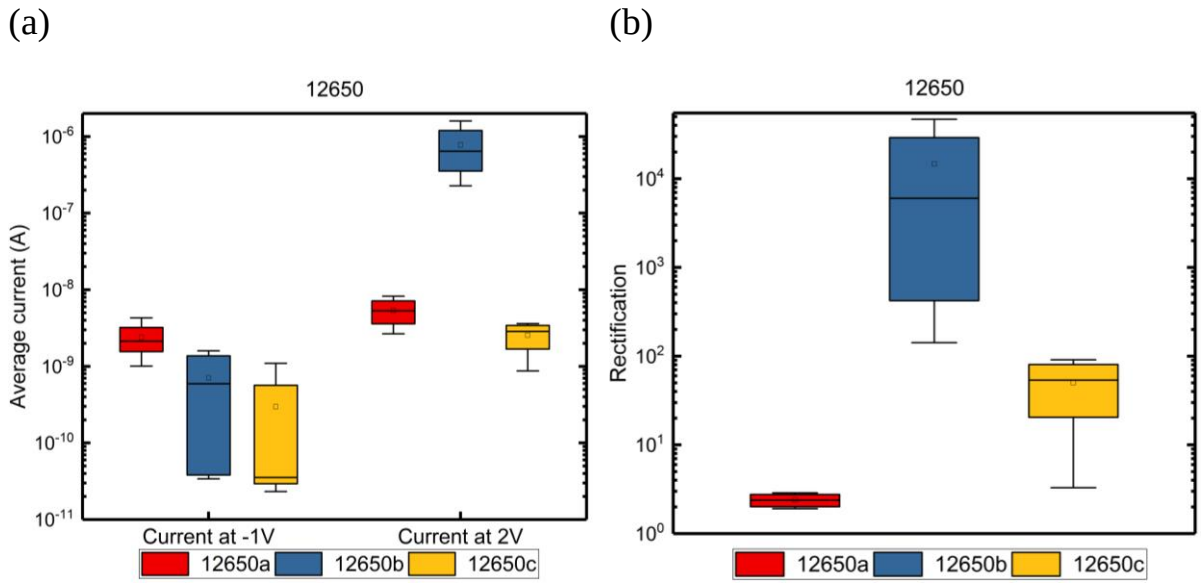

Figure 33: (a) Average currents taken at -1V and 2V for as-grown NWs (12650a, red boxes), NWs passivated with PO_x/Al_2O_3(12650b, blue boxes) and NWs passivated with SiO_2 (12650c, yellow boxes). (b) Ratio of forward current to leakage current (rectification) at 2V bias (data taken from a)).

6 Summary and Future work

In this thesis, we had the opportunity to work with three different sets of samples of InP NWs with embedded axial InAsP QDiscs. The objective was to investigate the effect of the number of QDiscs and the passivation impact on the optical and electrical properties. The ultimate goal was to better understand how to improve the performance of photodetectors based on large arrays of InP/InAsP arrays.

From optical measurements, we can conclude that:

- The PL emission intensity increases with the number of QDiscs.
- For samples with a single QDisc, 12648, POx/Al_2O_3passivation leads to an increase of the PL peak intensity for both InP and InAsP.
- For samples with multiple QDiscs, 12650, POx/Al_2O_3passivation shows good results on the InP PL peak intensity. On the other hand, both $POx/Al_2O_3$and SiO_2 passivation leads to a reduction in InAsP PL peak intensity.

From electrical measurements we found that:

- By increasing the number of QDiscs the reverse leakage current is increased, while the forward current is decreased. Thus, the electronic properties are not improved by increasing the number of QDiscs. It can be related to carrier recombination inside the QDiscs.
- For the samples with a single QDisc, passivation with SiO_2 seems better than Al_2O_3/PO_x for improving the I-V characteristics.
- For both samples with multiple QDiscs, 12649 and 12650, Al_2O_3/PO_x passivation gives a two order of magnitude improvement in rectification compared to as-grown NWs.

For future works, there is plenty of room for improvement of these promising NW heterostructures, which can be very important for optoelectronic devices like photodetectors, solar cells and LEDs. All the results obtained in this thesis work opens up a new set of interesting questions to be solved by systematic research. Questions such as which passivation layer optimizes the electro-optical properties of these heterostructure NWs or why the leakage/forward current is changed by passivation have to be answered by new sets of experiments. These include e.g. temperature-dependent PL, PLE (photoluminescence excitation spectroscopy) time-resolved PL and scanning probe spectroscopy. Moreover, the sample structure can be further optimized by e.g. growing pure crystal phase NWs, varying the number of QDiscs, improving the homogeneity and periodicity of the QDiscs and achieving proper control of the interface quality.

I hope that the data obtained in this work will be helpful for future improvement of InP/InAsP devices.

7 Popular scientific description

For the last decades, there has been a strong interest in scaling down electronics to improve performance and power consumption. This has led to miniaturization where device dimensions decrease to only a few tens of nanometers ($1\text{nm} = \frac{1}{1000\,000\,000}$ m). Scientists have discovered that materials and devices in nanometer sizes have different properties compared to bulk counterparts. One interesting nanostructure with important applications in electronics is semiconductor nanowires (NWs). Nanowires are thin needle-like structures with a diameter of 10 nm to a few 100 nm and a length of a few 100 nm to 100 μm. These nanostructures have demonstrated a great potential for being used in solar cells [1], photodetectors [2] and light emitting diodes (LED) [3]. They can be grown vertically directly on a substrate surface as seen in the enclosed figures. One advantage with the NWs is that different materials can be combined axially or radially in so called heterostructures. In this work we investigate InP/InAsP heterostructures, which are of great interest for high-speed electronic and photonic devices because of their tunable optical properties, excellent transport properties and low dark current.

More specifically, we investigate the effect of passivation of the surfaces of NWs. The performance of NW electronics is often limited by surface leakage due to the large surface-to-volume ratio of NWs. In order to improve the NW properties, we cover their surfaces with a special capping layer, called passivation layer. In this thesis work, the effect of surface passivation with two different materials (SiO_2 and PO_x/Al_2O_3) was studied. To evaluate the effect of the passivation on the electronic behavior, optical characterization (photoluminescence spectroscopy) and electrical measurements (nano-probe characterization) were carried out on single NWs and the results were compared. The results of this project will be used in the near future by scientists at NanoLund for optimization of solar cells and infrared photodetectors.

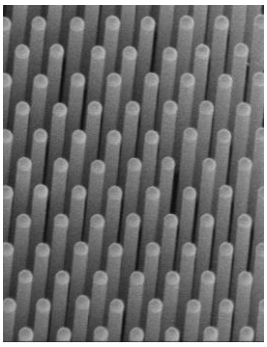

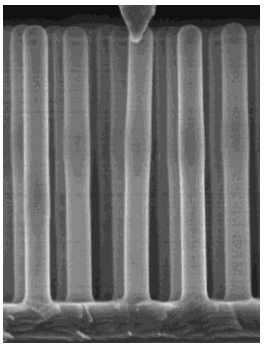

8 Appendix A

8.1 Quantization energies

Electrons	Bulk effective masses	Effective masses in InAsP QDisc
	$m^*_{InP} = 0.08m_0$	$m^*_{InAsP} = 0.47 \times 10^{-31} kg$
	$m^*_{InAs} = 0.023m_0$	
Holes		
heavy	$m^*_{InP} = 0.6m_0$	$m^*_{InAsP} = 4.596 \times 10^{-31} kg$
	$m^*_{InAs} = 0.41m_0$	
light	$m^*_{InP} = 0.089m_0$	$m^*_{InAsP} = 0.51 \times 10^{-31} kg$
	$m^*_{InAs} = 0.026m_0$	

Assumptions:

- QDisc group-V composition is taken as 50% As and 50% P
- Conduction band offset between InP and InAsP QDisc is taken as 0.35 eV
- Valence band offset between InP and InAsP QDisc is taken as 0.20 eV
- Interpolation for effective mass: $m^*_{InAsP} = \frac{m^*_{InAs} + m^*_{InP}}{2}$

Transition from VB to CB: $(E_g)_{QDisc} + E_{lh/hh} + E_{1e}$, $(E_g)_{QDisc} = 0.9\ eV$

Using the data above, I solve the Schrödinger eq. according to Ref. [51] for an InAsP QW embedded in InP by taking the barrier heights for electrons and holes equal to the respective band offset in the CB and VB. The quantization energies are given in the table below:

a=4nm	a=7nm	a=10nm
$E_{1e} = 0.142\ eV$	$E_{1e} = 0.0724\ eV$	$E_{1e} = 0.043\ eV$
$E_{hh} = 0.027\ eV$	E_{hh} =0.011 eV	$E_{hh} = 0.00589\ eV$
$E_{lh} = 0.102\ eV$	$E_{lh} = 0.057\ eV$	$E_{lh} = 0.035\ eV$

The table below shows the corresponding transition energies.

Transition from VB ground state to CB ground state		
a=4nm	a=7nm	a=10nm
lh to e1: 1.144 eV hh to e1: 1.069 eV	lh to e1: 1.029 eV hh to e1: 0.983 eV	lh to e1: 0.978 eV hh to e1: 0.949 eV

9 References

[1] J.Wallentin and et.al, "InP nanowire array solar cells achieving 13.8% efficiency by exceeding the ray optics limit," *Science,* vol. 339 (6123), p. 1057−1060, 2013.

[2] H.Pettersson and et.al, "Infrared Photodetectors in Heterostructure Nanowires," *Nano Lett.,* vol. 6(2), no. DOI: 10.1021/nl052170l, pp. 229-232, 2006.

[3] Y.Lifan and et.al, "Structural and Optical Properties of Disc-in-Wire InGaN/GaN LEDs," *Nano Lett.,* vol. 15, no. DOI: 10.1021/nl503826k, p. 1535–1539, 2015.

[4] C.P.Svensson and et.al, "Monolithic GaAs/InGaP nanowire light emitting diodes on silicon," *Nanotechnology,* vol. 19, no. Doi:10.1088/0957-4484/19/30/305201, p. 305201, 2008.

[5] R.R.LaPierre and et.al, "A review of III–V nanowire infrared photodetectors and sensors," *Appl. Phys,* vol. 50, no. Doi:10.1088/1361-6463/aa5ab3, p. 123001, 2017.

[6] D.M.Lyons and et.al, "Tailoring the Optical Properties of Silicon Nanowire Arrays through Strain," *Nano Letters,* vol. 2, no. DOI: 10.1021/nl0256098, p. 811–816, 2002.

[7] M.Karimi and et.al, "Room-temperature InP/InAsP Quantum Discs-in-Nanowire Infrared," *Nano letters,* p. 3356−3362, 2017.

[8] Y.Yang and et.al, "Coaxial Group III−Nitride Nanowire Photovoltaics," *Nano Lett.,* vol. 15 (5), no. DOI: 10.1021/nl900858v, p. 3541−3546, 2015.

[9] H.Zhu and et.al, "Nanowires: Building Blocks for Nanoscience and Nanotechnology," *Nat. Mater.,* vol. 14(6), p. 636−642, 2015.

[10] C.Soci and et.al, "Nanowire photodetectors," *Nanosci. Nanotechnol.,* vol. 10, p. 1430, 2010.

[11] V.J.Logeeswaran and et.al, "A perspective on nanowire photodetectors: current status, future challenges, and opportunities," *IEEE,* vol. 17, p. 1002, 2011.

[12] I.A.Goldthorpe and et.al, "Synthesis and Strain Relaxation of Ge-Core/Si-Shell Nanowire Arrays," *Nano Lett.,* vol. 8, no. DOI: 10.1021/nl802408y, p. 4081–4086, 2008.

[13] H.W.Shin and et.al, "Short-wavelength infrared photodetector on Si employing strain-induced growth of very tall InAs nanowire arrays," *Scientific report,* vol. 5, no. DOI: 10.1038/srep10764, 2015.

[14] Å. I and et.al, "A GaAs Nanowire Array Solar Cell With 15.3%," *IEEE,* vol. 6 (1), p. 185−190, 2016.

[15] J.P.Colinge and et.al, "Nanowire transistors without junctions," *Nature Nanotechnology,* vol. 5, no. DOI: 10.1038/NNANO.2010.15, pp. 225-229, 2010.

[16] K.J.Ryoung and et.al, "Schottky diodes based on a single GaN nanowire," *Nanotechnology,* vol. 13, p. 701–704, 2002.

[17] A.Berg and et.al, "Radial Nanowire Light-Emitting Diodes in the (AlxGa1–x)yIn1–yP Material System," *Nano Lett.,* vol. 16, no. DOI: 10.1021/acs.nanolett.5b04401, p. 656–662, 2016.

[18] M.R.Philip and et.al, "High efficiency green/yellow and red InGaN/AlGaN nanowire light-emitting diodes grown by molecular beam epitaxy," *Journal of Science: Advanced Materials and Devices,* vol. 2, no. https://doi.org/10.1016/j.jsamd.2017.05.009, pp. 150-155, 2017.

[19] D.Saxena and et.al, "Design and Room-Temperature Operation of GaAs/AlGaAs Multiple Quantum Well Nanowire Lasers," *Nano Lett.,* vol. 16, no. DOI: 10.1021/acs.nanolett.6b01973, p. 5080–5086, 2016.

[20] M.Karimi and et.al, "Intersubband Quantum Disc-in-Nanowire Photodetectors with Intersubband Quantum Disc-in-Nanowire Photodetectors with," *Nano Lett.,* vol. 18, no. DOI: 10.1021/acs.nanolett.7b04217, p. 365−372, 2018.

[21] X.Dai and et.al, "GaAs/AlGaAs Nanowire Photodetector," *Nano Lett.,* vol. 14 (5), no. DOI: 10.1021/nl5006004, p. 2688−2693, 2014.

[22] T.Haggren and et.al, "Strong surface passivation of GaAs nanowires with ultrathin InP and GaP capping layers," *Applied Physics Letters,* vol. 105, no. DOI: 10.1063/1.4891535, p. 033114, 2014.

[23] H.J.Joyce and et.al, "Electronic properties of GaAs, InAs and InP nanowires studied by terahertz spectroscopy," *Nanotechnology,* vol. 24, no. DOI:10.1088/0957-4484/24/21/214006, p.) 214006, 2013.

[24] O.Demiche and et.al, "Impact of surfaces on the optical properties of GaAs nanowires," *Applied Physics Letters,* vol. 97, no. DOI:10.1063/1.3519980, p. 201907, 2010.

[25] C.C.Chang and et.al, "Electrical and Optical Characterization of Surface Passivation in GaAs Nanowires," *Nano Lett.*, vol. 12, no. Doi.org/10.1021/nl301391h, p. 4484−4489, 2012.

[26] K.Lambert and et.al, "Increase of the Photoluminescence Intensity of InP Nanowires by Photoassisted Surface Passivation," *Journal of American Chemical Society*, vol. 127, no. DOI:10.1021/ja051860o, pp. 12357-12362, 2005.

[27] S.Münch and et.al, "Time-resolved photoluminescence investigations on HfO2-capped InP nanowires," *Nanotechnology*, vol. 21, no. DOIi:10.1088/0957-4484/21/10/105711, p. 105711 (7pp), 2010.

[28] V.Dhaka and et.al, "Protective capping and surface passivation of III-V nanowires by atomic layer deposition," *American Institute of Physics*, Vols. 6, 015016, no. Doi: 10.1063/1.4941063, 2016.

[29] Z.Zhong and et.al, *Nano Energy*, vol. 28, p. 106−114, 2016.

[30] L.E.Black and et.al, "Effective Surface Passivation of InP Nanowires by Atomic-Layer-Deposited Al2O3 with POx Interlayer," *Nano Lett.*, vol. 17, no. DOI: 10.1021/acs.nanolett.7b02972, p. 6287−6294, 2017.

[31] Y.Rosenwaks and et.al, *Phys. Rev. B: Condens. Matter Mater. Phys.*, vol. 44, p. 13097−13100., 1991.

[32] S.Bothra and et.al, "Surface recombination velocity and lifetime in InP measured by transient microwave reflectance," *IEEE Photovoltaic Spec. Conf.*, p. 404−408, 1990.

[33] C.A.Hoffman and et.al, *Appl. Phys. Lett.*, vol. 33, p. 536−539, 1978.

[34] X.Wang and et.al, . *IEEE Journal of Photovoltaics*, vol. 5, p. 282−287, 2015.

[35] C.Monier and et.al, "Band discontinuity in strained In(As,P)/InP heterostructures," *Applied Physics Letters*, vol. 72, no. DOI: 10.1063/1.121123, p. 1587, 1998.

[36] P.Desjardins and et.al, "Structural and optical properties of strain-relaxed InAsP/InP heterostructures grown by metalorganic vapor phase epitaxy on InP(001) using tertiarybutylarsine," *Journal of Applied Physics*, vol. 80, no. DOI: 10.1063/1.362921, p. 846, 1996.

[37] S.Perera and et.al, "Probing valence band structure in wurtzite InP nanowires using excitation spectroscopy," *App. Phys. Lett.*, vol. 97, no. DOI: 10.1063/1.3463036, p. 023106, 2010.

[38] L.V.Dao and et.al, "Time-resolved and time-integrated photoluminescence analysis of state filling and quantum confinement of silicon quantum dots," *Appl. Phys.*, vol. 97, no. DOI: 10.1063/1.1823027, p. 013501, 2005.

[39] J.Ciulik and M.R.Notis, "The Au/Sn phase diagram," *Journal of Alloys and Compounds*, vol. 191, no. DOI: 10.1016/0925-8388(93)90273-P, pp. 71-78, 1993.

[40] L.T.Gerben and et.al, "Valence Band Splitting in Wurtzite InP Nanowires Observed by Photoluminescence and Photoluminescence Excitation Spectroscopy," *Nano Research,* vol. 4, no. DOI 10.1007/s12274-010-0065-x, p. 159–163, 2011.

[41] H.Q.Hou and et.al, "Optical property of InAsP/InP strained quantum wells grown on InP (111)B and (100) substrates," *App.Phys.Lett.*, vol. 75, no. DOI: 10.1063/1.355920, p. 4673, 1994.

[42] A.Takayoshi and et.al, "Conduction-Band Discontinuity of InAsP/InP Heterojunction," *App.Phys.Lett,* vol. 37, pp. 3915-3918, 1998.

[43] N.Sköld and et.al, *Phys. Rev. B: Condens. Matter Mater. Phys.*, no. 041312, p. 80, 2009.

[44] L.E.Fröberg and et.al, *Nano Lett.*, vol. 8, no. 11, pp. 3815-3818, 2008.

[45] K.D.Thelander and et.al, "Controlling the Abruptness of Axial Heterojunctions in III−V Nanowires: Beyond the Reservoir Effect," *NanoLett,* vol. 12, no. DOI: 10.1021/nl301185x, p. 3200−3206, 2012.

[46] M.Heurlin and et.al, "In Situ Characterization of Nanowire Dimensions and Growth Dynamics by Optical Reflectance," *Nano Lett.*, vol. 15, no. DOI: 10.1021/acs.nanolett.5b01107, p. 3597–3602, 2015.

[47] M.H.M.Van.Weert and et.al, "Large redshift in photoluminescence of p-doped InP nanowires induced by Fermi-level pinning," *Appl. Phys. Lett.*, Vols. 88, 043109, 2006.

[48] K.Pemasiri and et.al, "Carrier Dynamics and Quantum Confinement in type II ZB-WZ InP Nanowire Homostructures," *Nano Lett.*, vol. 9, no. DOI: 10.1021/nl802997p, p. 648–654, 2009.

[49] G.Otnes and et.al, "Understanding InP Nanowire Array Solar Cell Performance by Nanoprobe-Enabled Single Nanowire Measurements," *NanoLett,* vol. 18, no. DOI: 10.1021/acs.nanolett.8b00494, p. 3038−3046, 2018.

[50] A.Darbandi and et.al, "Lithography-Free Fabrication of Core−Shell GaAs Nanowire Tunnel Diodes," *NanoLett,* vol. 15, no. DOI: 10.1021/acs.nanolett.5b01795, p. 5408−5413, 2015.

[51] J. H. Davies, "The physics od low-dimensional semiconductors," Cambridge University Press, 1998.

[52] A.Chitnis and et.al, "High-quality p–n junctions with quaternary AlInGaNÕInGaN quantum wells," *Appl. Phys. Lett.,* vol. 77, no. DOI: 10.1063/1.1331084, p. 3800, 2000.

[53] V.K.Dixit and et.al, "A versatile phenomenological model for the S-shaped temperature dependence of photoluminescence energy for an accurate determination of the exciton localization energy in bulk and quantum well structures," *Applied Physics,* vol. 47, no. DOI:10.1088/0022-3727/47/6/065103, p. 065103 (14pp), 2014.

[54] Dierschke and et.al, "Forward and Reverse Tunnel Currents in Gallium Phosphide Diffused p-n Junctions," *App. Phys.,* vol. 41, no. DOI: 10.1063/1.1658343, p. 329, 1970.

[55] J.M.Shah and et.al, "Experimental analysis and theoretical model for anomalously high ideality factors „nš2.0… in AlGaNÕGaN p-n junction diodes," *JOURNAL OF APPLIED PHYSICS,* vol. 94, no. DOI: 10.1063/1.1593218, p. 2627, 2003.

[56] N.Tajik and et.al, "Photoluminescence model of sulfur passivated p-InP nanowires," *Nanotechnology,* vol. 21, no. DOI:10.1088/0957-4484/23/31/315703, pp. 315703-315709, 2012.

[57] T.Mårtensson and et.al, "Nanowire Arrays Defined by Nanoimprint Lithography," *Nano Lett.,* vol. 4, no. DOI: 10.1021/nl035100s, p. 699–702, 2004.

[58] V.Jain and et.al, "Study of photocurrent generation in InP nanowire-based p(+)-i-n(+) photodetectors," *Nano Reseach,* vol. 7, no. DOI: 10.1007/s12274-014-0422-2, pp. 544-552, 2014.